J|A|C|S
ARTICLES
Published on Web 04/03/2007

Large Ground-State Entropy Changes for Hydrogen Atom Transfer Reactions of Iron Complexes

Elizabeth A. Mader, Ernest R. Davidson, and James M. Mayer*

Contribution from the University of Washington, Campus Box 351700, Seattle, Washington 98195-1700

Received December 4, 2006; E-mail: mayer@chem.washington.edu

Abstract: Reported herein are the hydrogen atom transfer (HAT) reactions of two closely related dicationic iron tris(α-diimine) complexes. $Fe^{II}(H_2bip)$ (iron(II) tris[2,2′-bi-1,4,5,6-tetrahydropyrimidine]diperchlorate) and $Fe^{II}(H_2bim)$ (iron(II) tris[2,2′-bi-2-imidazoline]diperchlorate) both transfer H• to TEMPO (2,2,6,6-tetramethyl-1-piperidinoxyl) to yield the hydroxylamine, TEMPO-H, and the respective deprotonated iron(III) species, $Fe^{III}(Hbip)$ or $Fe^{III}(Hbim)$. The ground-state thermodynamic parameters in MeCN were determined for both systems using both static and kinetic measurements. For $Fe^{II}(H_2bip)$ + TEMPO, $\Delta G^\circ = -0.3 \pm 0.2$ kcal mol^{-1}, $\Delta H^\circ = -9.4 \pm 0.6$ kcal mol^{-1}, and $\Delta S^\circ = -30 \pm 2$ cal mol^{-1} K^{-1}. For $Fe^{II}(H_2bim)$ + TEMPO, $\Delta G^\circ = 5.0 \pm 0.2$ kcal mol^{-1}, $\Delta H^\circ = -4.1 \pm 0.9$ kcal mol^{-1}, and $\Delta S^\circ = -30 \pm 3$ cal mol^{-1} K^{-1}. The large entropy changes for these reactions, $|T\Delta S^\circ| = 9$ kcal mol^{-1} at 298 K, are exceptions to the traditional assumption that $\Delta S^\circ \approx 0$ for simple HAT reactions. Various studies indicate that hydrogen bonding, solvent effects, ion pairing, and iron spin equilibria do not make major contributions to the observed ΔS°_{HAT}. Instead, this effect arises primarily from changes in vibrational entropy upon oxidation of the iron center. Measurement of the electron-transfer half-reaction entropy, $|\Delta S^\circ_{Fe(H2bim)/ET}| = 29 \pm 3$ cal mol^{-1} K^{-1}, is consistent with a vibrational origin. This conclusion is supported by UHF/6-31G* calculations on the simplified reaction $[Fe^{II}(H_2N{=}CHCH{=}NH_2)_2(H_2bim)]^{2+}\cdots ONH_2 \leftrightarrows [Fe^{II}(H_2N{=}CHCH{=}NH_2)_2(Hbim)]^{2+}\cdots HONH_2$. The discovery that ΔS°_{HAT} can deviate significantly from zero has important implications on the study of HAT and proton-coupled electron-transfer (PCET) reactions. For instance, these results indicate that free energies, rather than enthalpies, should be used to estimate the driving force for HAT when transition-metal centers are involved.

Introduction

Hydrogen atom transfer (HAT) is one of the most common and fundamental chemical reactions (eq 1). It is a cornerstone

$$A{-}H + B^\bullet \rightarrow A^\bullet + H{-}B \qquad (1)$$

of organic free-radical chemistry, from combustion to the action of antioxidants both in vitro and in vivo.[1] HAT can be defined as the concerted movement of a proton and an electron ($e^- + H^+ \equiv H^\bullet$) in a single kinetic step where both the proton and the electron originate from the same reactant and travel to the same product. HAT is one type of the broad class of proton-coupled electron-transfer (PCET) reactions, which also includes reactions where the proton and electron are separated.[2−6] In recent years, it has become clear that HAT involving transition-metal species is very common, occurring in discrete metal complexes, metalloprotein active sites, and, most likely, sites on metal oxide surfaces.[2−4,7,8] Among the many metalloenzymes that utilize HAT reactions are lipoxygenases,[9] ribonucleotide reductases,[3b,7a] and methane monooxygenases.[10]

(1) (a) Ingold, K. U. In *Free Radicals*; Kochi, J. K., Ed.; Wiley: New York, 1973; Vol. 1, Chapter 2, p 67ff; Russell, G. A. In *Free Radicals*; Kochi, J. K., Ed.; Wiley: New York, 1973; Vol. 1, Chapter 7, pp 275−331; O'Neal, H.; Benson, S. W. In *Free Radicals*; Kochi, J. K., Ed.; Wiley: New York, 1973; Vol. 2, Chapter 17, pp 275−359. (b) *Radical Reaction Rates in Liquids*, Landolt−Börnstein New Series; Fischer, H., Ed.; Springer-Verlag: Berlin, 1984; Vol. 13, Subvols. a-e; *Radical Reaction Rates in Liquids*, Landolt−Börnstein New Series; Fischer, H., Ed.; Springer-Verlag: Berlin, 1994; Vol. 18, Subvols. A−E. (c) Hendry, D. G.; Mill, T.; Piszkiewicz, L.; Howard, J. A.; Eigenmann, H. K. *J. Phys. Chem. Ref. Data* **1974**, *3*, 937−978. (d) Fossey, J.; Lefort, D.; Sorba, J. *Free Radicals in Organic Chemistry*; Wiley: New York, 1995. (e) Leffler, J. E. *An Introduction to Free Radicals*; Wiley: New York, 1993; Chapters 7−8. (f) Halliwell, B.; Gutteridge, J. M. C. *Free Radicals in Biology and Medicine*; Oxford University Press: New York, 1999. (g) *Oxidative Stress: Oxidants and Antioxidants*; Sies, H., Ed.; Academic: New York, 1991. (h) *Active Oxygen in Chemistry*; Foote, C. S., Valentine, J. S., Liebman, J., Greenberg, A., Eds.; Blackie, Chapman and Hall: Glasgow, 1995.

(2) (a) Mayer, J. M. *Annu. Rev. Phys. Chem.* **2004**, *55*, 363−390. (b) Mayer, J. M.; Rhile, I. J. *Biochim. Biophys. Acta* **2004**, *1655*, 51−58. (c) Mayer, J. M.; Rhile, I. J.; Larsen, F. B.; Mader, E. A.; Markle, T. F.; DiPasquale, A. G. *Photosynth. Res.* **2006**, *87*, 3−20; Mayer, J. M.; Rhile, I. J.; Larsen, F. B.; Mader, E. A.; Markle, T. F.; DiPasquale, A. G. *Photosynth. Res.* **2006**, *87*, 21−24. (d) Mayer, J. M.; Mader, E. A.; Roth, J. P.; Bryant, J. R.; Matsuo, T.; Dehestani, A.; Bales, B. C.; Watson, E. J.; Osako. T.; Valliant-Saunders, K.; Lam, W.-H.; Hrovat, D. A.; Borden, W. T.; Davidson, E. R. *J. Mol. Catal. A: Chem.* **2006**, *251*, 24−33.

(3) (a) Cukier, R. I.; Nocera, D. G. *Annu. Rev. Phys. Chem.* **1998**, *49*, 337−369. (b) Stubbe, J.; Nocera, D. G.; Yee, C. S.; Chang, M. C. Y. *Chem. Rev.* **2003**, *103*, 2167−2201. (c) Meyer, T. J.; Huynh, M. H. V. *Inorg. Chem.* **2003**, *42*, 8140−8160. (d) Lebeau, E. L.; Binstead, R. A.; Meyer, T. J. *J. Am. Chem. Soc.* **2001**, *123*, 10535−10544.

(4) (a) Hammes-Schiffer, S. *Acc. Chem. Res.* **2001**, *34*, 273−281. (b) Cukier, R. I. *J. Phys. Chem. B* **2002**, *106*, 1746−1757. (c) Kuznetsov, A. M.; Ulstrup, J. *Can. J. Chem.* **1999**, *77*, 1085−1096. (d) Krishtalik, L. I. *Biochim. Biophys. Acta* **2000**, *1458*, 6−27. (e) Hatcher, E.; Soudackov, A.; Hammes-Schiffer, S. *Chem. Phys.* **2005**, *319*, 93−100. (f) Cukier, R. I. *Molecular Bioenergetics*; ACS Symposium Series 883; American Chemical Society: Washington, DC, 2004; pp 145−158.

For more than 70 years, numerous HAT reactions have been measured and understood using the Bell−Evans−Polanyi equation (eq 2). This equation correlates the activation energy, E_a, with the enthalpic driving force of the reaction (ΔH) using two parameters (α, β) that are specific to a set of reactions rather than to all HATs.[11,12] Using this thermochemical perspective (rather than one based on electronic structure), we have found strong analogies between organic and metal-mediated HAT reactions.[13,14] Under standard conditions, the ΔH for a HAT reaction is simply the difference between the bond dissociation enthalpies (BDEs) of AH and BH (eq 3). The correlation indicated by eqs 2 and 3 is one of the primary historical reasons why chemists are so focused on BDEs (for instance, why tables of BDEs appear in many organic chemistry texts).

$$E_a = \alpha(\Delta H) + \beta \quad (2)$$

$$\Delta H^\circ = \mathrm{BDE(AH)} - \mathrm{BDE(BH)} \quad (3)$$

Like the Polanyi equation, Marcus Theory correlates activation barriers with driving force, but the Marcus approach uses free energies rather than enthalpies.[17] It was developed for electron-transfer (ET) reactions but has been applied to transfers of protons, hydrides, and other groups.[15] Recently, we have shown that a wide range of HAT rate constants can be understood and predicted using Marcus Theory, specifically the Marcus cross relation (eq 4).[14,16] The rate constant of HAT from AH to B$^\bullet$ (eq 1, k_{AB}) is related to the equilibrium constant, K_{AB},

$$k_{AB} = \sqrt{k_{AA} k_{BB} K_{AB} f} \quad (4)$$

as well as the rate constants of the component-degenerate HAT self-exchange reactions (AH + A$^\bullet$ → A$^\bullet$ + HA; k_{AA}). The frequency factor, f, is usually close to unity.[17] This treatment has been successfully applied to reactions of C−H, N−H, and O−H bonds, including both metal and organic compounds, although there are exceptions.[14]

The difference between the Polanyi correlation with ΔH° and the Marcus treatment with ΔG° has not been of serious concern because HAT reactions are typically assumed to have ground-state entropies of reaction close to zero.[18] When $\Delta S^\circ \approx 0$, $\Delta G^\circ \approx \Delta H^\circ = \Delta$BDE. Assuming $\Delta S^\circ \approx 0$ seems reasonable because these reactions do not involve a change in the number of molecules or their charge or overall size. For analogous reasons, AH and A$^\bullet$ are often assumed to have similar entropies so that ΔS° for bond homolysis (A−H → A$^\bullet$ + H$^\bullet$) is very close to S°(H$^\bullet$). This is also a key assumption in the increasingly common determination of BDEs from solution pK_a and $E_{1/2}$ values, as discussed in more detail below.[19−24]

Described here are detailed studies of HAT reactions involving iron complexes (eqs 5 and 6) that have large entropies of reaction, $|\Delta S^\circ| \approx 30$ cal K^{-1} mol^{-1}. A preliminary report on eq 5 emphasized its negative activation enthalpy ($\Delta H^\ddagger$) and its

(5) (a) Biczók, L.; Gupta, N.; Linschitz, H. *J. Am. Chem. Soc.* **1997**, *119*, 12601−12609. (b) Sjödin, M.; Ghanem, R.; Polivka, T.; Pan, J.; Styring, S.; Sun, L.; Sundström, V.; Hammarström, L. *Phys. Chem. Chem. Phys.* **2004**, *6*, 4851−4858. (c) Reece, S. Y.; Nocera, D. G. *J. Am. Chem. Soc.* **2005**, *127*, 9448−9458. (d) Costentin, C.; Evans, D. H.; Robert, M.; Savéant, J.-M.; Singh, P. S. *J. Am. Chem. Soc.* **2005**, *127*, 12490−12491. (e) Rhile, I. J.; Markle, T. F.; Nagao, H.; DiPasquale, A. G.; Lam, O. P.; Lockwood, M. A.; Rotter, K.; Mayer, J. M. *J. Am. Chem. Soc.* **2006**, *128*, 6075−6088. (f) Fecenko, C. J.; Meyer, T. J.; Thorp, H. H. *J. Am. Chem. Soc.* **2006**, *128*, 11020−11021.

(6) (a) Mayer, J. M.; Hrovat, D.; Thomas, J. L.; Borden, W. T. *J. Am. Chem. Soc.* **2002**, *124*, 11142−11147. (b) Lingwood, M.; Hammond, J. R.; Hrovat, D. A.; Mayer, J. M.; Borden, W. T. *J. Chem. Theory Comput.* **2006**, *2*, 740−745. (c) Pratt, D. A.; Blake, J. A.; Mulder, P.; Walton, J. C.; Korth, H.-G.; Ingold, K. U. *J. Am. Chem. Soc.* **2004**, *126*, 10667−10675.

(7) (a) Stubbe, J.; van der Donk, W. A. *Chem. Rev.* **1998**, *98*, 705−762. (b) Pesavento, R. P.; van der Donk, W. A. *Adv. Protein Chem.* **2001**, *58*, 317−385. (c) Marsh, E. N. G. *BioEssays* **1995**, *17*, 431−441. (d) Pierre, J.-L.; Thomas, F. *C. R. Chim.* **2005**, *8*, 65−74. (e) Fontecave, M.; Pierre, J.-L. *C. R. Acad. Sci., Ser. IIc: Chim.* **2001**, *4*, 531−538. (f) Decker, A.; Chow, M. S.; Kemsley, J. N.; Lehnert, N.; Solomon, E. I. *J. Am. Chem. Soc.* **2006**, *128*, 4719−4733.

(8) (a) Labinger, J. A. *J. Mol. Catal. A: Chem.* **2004**, *220*, 27−35. (b) Labinger, J. A. *Catal. Lett.* **1988**, *1*, 371−375.

(9) (a) Liang, Z.-X.; Klinman, J. P. *Curr. Opin. Struct. Biol.* **2004**, *14*, 648−655. (b) Hatcher, E.; Soudackov, A. V.; Hammes-Schiffer, S. *J. Am. Chem. Soc.* **2004**, *126*, 5763−5775. (c) Lehnert, N.; Solomon, E. I. *J. Biol. Inorg. Chem.* **2003**, *8*, 294−305. (d) Goldsmith, C. R.; Stack, T. D. P. *Inorg. Chem.* **2006**, *45*, 6048−6055.

(10) (a) Ragsdale, S. W. *Chem. Rev.* **2006**, *106*, 3317−3337. (b) Baik, M.-H.; Newcomb, M.; Friesner, R. A.; Lippard, S. J. *Chem. Rev.* **2003**, *103*, 2385−2419. (c) Brazeau, B. J.; Austin, R. N.; Tarr, C.; Groves, J. T.; Lipscomb, J. D. *J. Am. Chem. Soc.* **2001**, *123*, 11831−11837.

(11) (a) Shaik, S. S.; Schlegel, H. B.; Wolfe, S. *Theoretical Aspects of Physical Organic Chemistry: The S_N2 Reaction*; John Wiley & Sons, Inc.: New York, 1992; pp 11−23. (b) Knox, J. H. Rate Constants in the Gas-Phase Oxidation of Alkanes and Alkyl Radicals. In *Oxidation of Organic Compounds*; Mayo, F. R., Ed.; Advances in Chemistry Series 76 (II); American Chemical Society: Washington, DC, 1968; pp 1−22. (c) References 1a,d,e.

(12) Equation 2 is not limited to standard states; therefore, ΔH rather than ΔH° is used. Bond dissociation energies are ΔH° values and are defined at 298 K and 1 atm (gas-phase BDEs) or unit activity standard state ([assumed 1 M] for solution BDEs).

(13) Mayer, J. M. *Acc. Chem. Res.* **1998**, *31*, 441−450.

(14) Roth, J. P.; Yoder, J. C.; Won, T.-J.; Mayer, J. M. *Science* **2001**, *294*, 2524−2526.

(15) (a) Albery, W. J. *Annu. Rev. Phys. Chem.* **1980**, *31*, 227−263. (b) Kristjánsdóttir, S. S.; Norton, J. R. *J. Am. Chem. Soc.* **1991**, *113*, 4366−4367. (c) Guthrie, J. P. *J. Am. Chem. Soc.* **1997**, *119*, 1151−1152. (d) Lee, I.-S. H.; Jeoung, E. H.; Kreevoy, M. M. *J. Am. Chem. Soc.* **1997**, *119*, 2722−2728 and references therein. (e) Lewis, E. S.; Hu, D. D. *J. Am. Chem. Soc.* **1984**, *106*, 3292−3296. (f) Pellerite, M. J.; Brauman, J. I. *J. Am. Chem. Soc.* **1983**, *105*, 2672−2680. (g) Shea, T. M.; Deraniyagala, S. P.; Studebaker, D. B.; Westmoreland, T. D. *Inorg. Chem.* **1996**, *35*, 7699−7703. (h) Anderson, K. A.; Kirchner, K.; Dodgen, H. W.; Hunt, J. P.; Wherland, S. *Inorg. Chem.* **1992**, *31*, 2605−2608. (i) Reference 11a.

(16) Mader, E. A.; Larsen, A. S.; Mayer, J. M. *J. Am. Chem. Soc.* **2004**, *126*, 8066−8067.

(17) (a) Marcus, R. A.; Sutin, N. *Biochim. Biophys. Acta* **1985**, *811*, 265−322. (b) Sutin, N. *Prog. Inorg. Chem.* **1983**, *30*, 441.

(18) Blanksby, S. J.; Ellison, G. B. *Acc. Chem. Res.* **2003**, *36*, 255−263.

(19) (a) Wiberg, K. B.; Foster, G. *J. Am. Chem. Soc.* **1961**, *83*, 423−429; thermochemical cycle is on p 425. (b) Eberson, L. *Acta Chem. Scand.* **1963**, *17*, 2004−2018. (c) Jaun, B.; Schwarz, J.; Breslow, R. *J. Am. Chem. Soc.* **1980**, *102*, 5741−5748 and references therein.

(20) Leading references: (a) Bordwell, F. G.; Cheng, J.-P.; Ji, G.-Z.; Satish, A. V.; Zhang, X. *J. Am. Chem. Soc.* **1991**, *113*, 9790−9795. (b) Bordwell, F. G.; Cheng, J.-P.; Harrelson, J. A., Jr. *J. Am. Chem. Soc.* **1988**, *110*, 1229−1231. (c) Bordwell, F. G.; Satish, A. V.; Zhang, S.; Zhang, X.-M. *Pure Appl. Chem.* **1995**, *67*, 735−740. (d) Bordwell, F. G.; Liu, W.-Z. *J. Am. Chem. Soc.* **1996**, *118*, 10819−10823.

(21) A subset of the references in this area are: (a) Anne, A.; Fraoua, S.; Grass, V.; Moiroux, J.; Savéant, J.-M. *J. Am. Chem. Soc.* **1998**, *120*, 2951−2958. (b) Koshino, N.; Cai, Y.; Espenson, J. H. *J. Phys. Chem. A.* **2003**, *107*, 4262−4267. (c) Cheng, J.-P.; Liu, B.; Zhao, Y.; Wen, Z.; Sun, Y. *J. Am. Chem. Soc.* **2000**, *122*, 9987−9992.

(22) A subset of the references using BDEs are: (a) Parker, V. D.; Handoo, K. L.; Roness, F.; Tilset, M. *J. Am. Chem. Soc.* **1991**, *113*, 7493−7498. (b) Tilset, M.; Parker, V. D. *J. Am. Chem. Soc.* **1990**, *112*, 2843. (c) Tilset, M.; Parker, V. D. *J. Am. Chem. Soc.* **1989**, *111*, 6711−6717. (d) Borovik, A. S. *Acc. Chem. Res.* **2005**, *38*, 54−61. (e) Zhang, J.; Grills, D. C.; Huang, K.-W.; Fujita, E.; Bullock, R. M. *J. Am. Chem. Soc.* **2005**, *127*, 15684−15685. (f) Carrell, T. G.; Bourles, E.; Lin, M.; Dismukes, G. C. *Inorg. Chem.* **2003**, *42*, 2849−2858. (g) Astruc, D. *Acc. Chem. Res.* **2000**, *33*, 287−298. (h) Wang, D.; Angelici, R. J. *J. Am. Chem. Soc.* **1996**, *118*, 935−942. (i) Eisenberg, D. C.; Norton, J. R. *Isr. J. Chem.* **1991**, *31*, 55−66. (j) Simões, J. A. M.; Beauchamp, J. L. *Chem. Rev.* **1990**, *90*, 629−688. (k) Reference 61b.

(23) (a) Wayner, D. D. M.; Parker, V. D. *Acc. Chem. Res.* **1993**, *26*, 287−294 and references therein. (b) Tang, L.; Papish, E. T.; Abramo, G. P.; Norton, J. R.; Baik, M.-H.; Friesner, R. A.; Rappe, A. *J. Am. Chem. Soc.* **2003**, *125*, 10093−10102; Tang, L.; Papish, E. T.; Abramo, G. P.; Norton, J. R.; Baik, M.-H.; Friesner, R. A.; Rappe, A. *J. Am. Chem. Soc.* **2006**, *128*, 11314.

(24) For a few studies using BDFEs, see: (a) Fu, X.; Wayland, B. B. *J. Am. Chem. Soc.* **2005**, *127*, 16460−16467 and references therein. (b) Miedaner, A.; Raebiger, J. W.; Curtis, C. J.; Miller, S. M.; DuBois, D. L. *Organometallics* **2004**, *23*, 2670−2679. (c) Ellis, W. W.; Miedaner, A.; Curtis, C. J.; Gibson, D. H.; DuBois, D. L. *J. Am. Chem. Soc.* **2002**, *124*, 1926−1932.

Table 1. Selected Bond Lengths (Å) and Angles (deg) for **$Fe^{III}(H_2bip)$** and **$Fe^{n}(H_xbim)$** Structures[a]

	$Fe^{III}(H_2bip)$[b]	$Fe^{III}(H_2bim)$[c,d]	$Fe^{III}(Hbim)$[c,e]	$Fe^{II}(H_2bim)$[c,f,g]
Fe−N(1)	1.959(3)	2.090(7)	2.121(3)	2.172(3)
Fe−N(3)	1.954(3)	2.080(7)	2.076(3)	2.198(4)
Fe−N(5)	1.958(3)	2.079(7)	2.151(4)	
Fe−N(6)	1.962(3)	2.064(7)	2.084(3)	
Fe−N(9)	1.960(3)	2.075(7)	2.005(4)[h]	
Fe−N(11)	1.954(3)	2.085(7)	2.121(4)	2.167(3)
∠N(1)−Fe−N(3)	81.21(14)	77.3(3)	77.0(1)	75.7(1)
∠N(5)−Fe−N(6)	81.14(14)	77.3(3)	76.5(1)	
∠N(9)−Fe−N(11)	81.43(14)	77.2(3)	78.4(2)	76.4(2)[g]
∠N(1)−Fe−N(9)	176.98(15)	165.3(3)	167.4(2)	
∠N(3)−Fe−N(6)	173.87(14)	163.1(3)	164.4(2)	171.4(2)[i]
∠N(5)−Fe−N(11)	176.22(13)	167.3(1)	164.3(1)	166.6(1)[j]

[a] Numbering refers to **$Fe^{III}(H_2bip)$** structure. [b] Data collected at 130 K. [c] Reference 27. [d] Data collected at 161 K. [e] Data collected at 298 K. [f] Data collected at 300 K. [g] **$Fe^{II}(H_2bim)$** has a crystallographic mirror plane, N(11)−Fe−N(11A). [h] This N(9) is in the same ring as the deprotonated nitrogen. [i] ∠N(3)−Fe−N(3A). [j] ∠N(1)−Fe−N(11).

quantitative prediction by the Marcus cross relation (eq 4).[16] The large entropy change in reactions 5 and 6 is equivalent to a change in equilibrium constant of 4×10^6 ($\Delta \ln K_{eq} = \Delta S°/R$) and contributes $|T\Delta S°| = 9$ kcal mol^{-1} to the free energy of reaction at 298 K. In this system, BDEs calculated from pK_a and $E_{1/2}$ values with the assumption that $S°(A^{\bullet}) \approx S°(AH)$ are in error by 9 kcal mol^{-1}. The success of the Marcus treatment demonstrates that these reactions should be analyzed using free energies rather than enthalpies as in the traditional Polanyi equation (eq 2). Herein, we explore the origin of this large entropy change using both experiment and theory and discuss the implications of the large $|\Delta S°|$.

Results

The HAT reactions of two closely related iron(II) tris(α-diimine) complexes have been studied, $[Fe^{II}(H_2bip)_3]^{2+}$ (**$Fe^{II}(H_2bip)$**, H_2bip = 2,2′-bi-1,4,5,6-tetrahydropyrimidine) and $[Fe^{II}(H_2bim)_3]^{2+}$ (**$Fe^{II}(H_2bim)$**, H_2bim = 2,2′-bi-2-imidazoline). **$Fe^{II}(H_2bip)$** and **$Fe^{II}(H_2bim)$** react rapidly at room temperature with the stable nitroxyl TEMPO in anaerobic acetonitrile to give the hydroxylamine TEMPO-H and the deprotonated iron(III) complex, $[Fe^{III}(H_2bip)(Hbip)]^{2+}$ (**$Fe^{III}(Hbip)$**) or $[Fe^{III}(H_2bim)(Hbim)]^{2+}$ (**$Fe^{III}(Hbim)$**) (eqs 5 and 6).[14,16] The reaction is net HAT to the organic radical by the concerted transfer of one proton (from the ligand) and one electron (from oxidation of the iron). In these equations, the two ancillary ligands denoted by N−N are the same as the ligand, L, drawn in full for the respective Fe(II) complexes (H_2bip or H_2bim). The iron complexes are of the general form **$Fe^{n}(H_xL)$**, where *n* is the oxidation state of the iron and where *x* indicates the protonation state of the ligand.

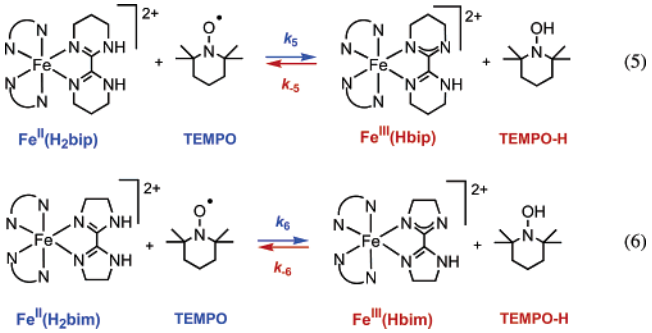

I. Characterization. The four iron species in eqs 5 and 6 have been previously reported,[25,26] including crystal structures for **$Fe^{II}(H_2bim)$**, **$Fe^{III}(Hbim)$**, and the fully protonated $[Fe^{III}(H_2bim)_3][ClO_4]_3$ (**$Fe^{III}(H_2bim)$**).[27] While structures of **$Fe^{II}(H_2bip)$** or **$Fe^{III}(Hbip)$** are not available, X-ray-quality crystals of the fully protonated iron(III) species, $[Fe^{III}(H_2bip)_3][(ClO_4)_3]$ (**$Fe^{III}(H_2bip)$**), have been obtained from MeCN/Et_2O (Tables 1and S5; Figure 1A). The structure contains a standard pseudo-D_{3d} tris(chelate) ion whose NH protons are hydrogen bonded to the perchlorate counterions, similar to all three of the **$Fe^{n}(H_xbim)$** complexes, Table 2. The three H_2bip ligands in **$Fe^{III}(H_2bip)$** have similar diimine bite angles, N−Fe−N = 81.3 ± 0.2°, but their N−C−C−N torsion angles vary by >10°. The distortion minimizes steric interactions between the chair conformations of the H_2bip ligands. This is in contrast to the three **$Fe^{n}(H_xbim)$** complexes, which have essentially planar ligands (N−C−C−N torsion <0.06°).

The Fe−N distances in **$Fe^{III}(H_2bip)$** range from 1.954(3) to 1.962(3) Å. These are indicative of a low-spin iron(III) center, consistent with structures of related Fe(III) diimines.[28,29] Solid-state magnetic measurements[26a] have shown that **$Fe^{III}(H_2bip)$** is low spin at 100 K (the X-ray data collection temperature) and undergoes a gradual spin-state transition from 200 to 400 K. **$Fe^{III}(Hbip)$** and **$Fe^{II}(H_2bip)$** behave similarly.[26] In contrast, the three analogous **$Fe^{n}(H_xbim)$** complexes are exclusively high-spin above 120 K[26] (the structure of **$Fe^{III}(H_2bim)$** discussed here was obtained at 161 K). This difference in spin-state is consistent with the Fe−N distances in **$Fe^{III}(H_2bip)$** being, on average, 0.12 Å shorter than those in **$Fe^{III}(H_2bim)$**.[28b] In Fe(III) complexes, the distances d(Fe−N) are typically ∼0.12 Å shorter for low-spin versus those for high-spin complexes; for Fe(II), the effect is slightly larger, as Δd(Fe−N) ∼ 0.2 Å.[28b] In addition, we observe a ca. 0.1 Å difference between bond distances for high-spin Fe(III) versus that for high-spin Fe(II).

(25) Yoder, J. C.; Roth, J. P.; Gussenhoven, E. M.; Larsen, A. S.; Mayer, J. M. *J. Am. Chem. Soc.* **2003**, *125*, 2629−2640.
(26) (a) Burnett, M. G.; McKee, V.; Nelson, S. M. *J. Chem. Soc., Dalton Trans.* **1981**, 1492−1497. (b) Burnett, M. G.; McKee, V.; Nelson, S. M. *J. Chem. Soc., Chem. Commun.* **1980**, 599−601. (c) Wang, J. C.; Bauman, J. E., Jr. *Inorg. Chem.* **1965**, *4*, 1613−1615.
(27) Roth, J. P.; Lovell, S.; Mayer, J. M. *J. Am. Chem. Soc.* **2000**, *122*, 5486−5498.
(28) (a) van Koningsbruggen, P. J.; Maeda, Y.; Oshio, H. *Top. Curr. Chem.* **2004**, *233*, 259−324. (b) Gutlich, P.; Goodwin, A. H. *Top. Curr. Chem.* **2004**, *233*, 1−47. (c) Konig, E. *Struct. Bonding* **1991**, *76*, 51−152.
(29) (a) Sunatsuki, Y.; Ohta, H.; Kojima, M.; Ikuta, Y.; Goto, Y.; Matsumoto, N.; Iijima, S.; Akashi, H.; Kaizaki, S.; Dahan, F.; Tuchagues, J.-P. *Inorg. Chem.* **2004**, *43*, 4154−4171. (b) Maroney, M. J.; Fey, E. O.; Baldwin, D. A.; Stenkamp, R. E.; Jensen, L. H.; Rose, N. J. *Inorg. Chem.* **1986**, *25*, 1409−1414. (c) Saha, N. C.; Butcher, R. J.; Chaudhuri, S.; Saha, N. *Polyhedron* **2003**, *22*, 375−381. (d) Endicott, J. F.; Durham, B.; Glick, M. D.; Anderson, T. J.; Kuszaj, J. M.; Schmonsees, W. G.; Balakrishnan, K. P. *J. Am. Chem. Soc.* **1981**, *103*, 1431−1440.

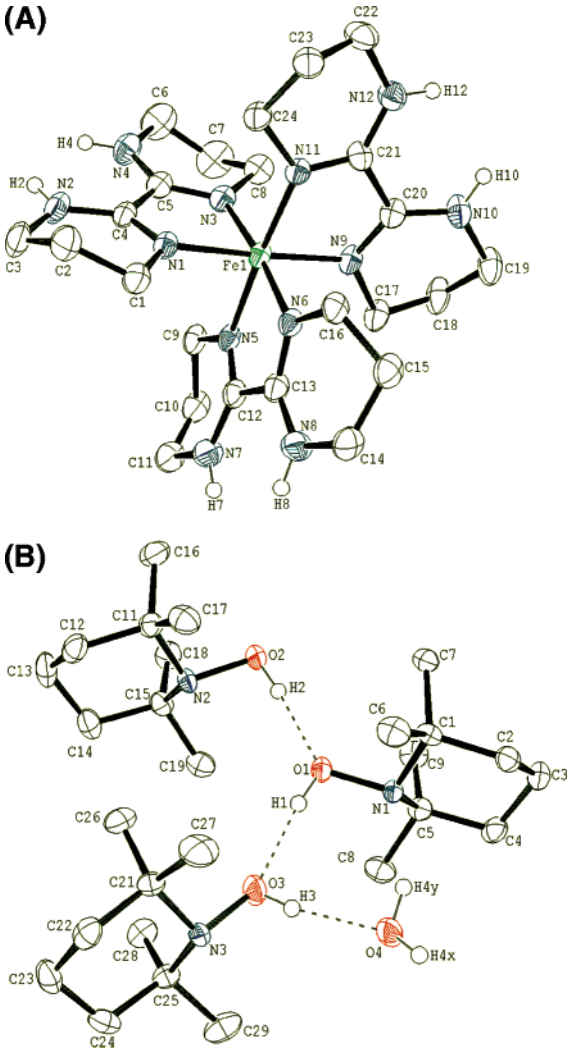

Figure 1. ORTEPs of (A) the cation in $Fe^{III}(H_2bip)_3(ClO_4)_3 \cdot MeCN \cdot Et_2O$ and (B) the unit cell of TEMPO-H$\cdot^1/_3H_2O$. Thermal ellipsoids are drawn at 50% probability; only the hydrogen atoms bound to N or O are shown.

The literature preparation of TEMPO-H by dithionite reduction of TEMPO[30] has been improved, and an X-ray structure has been obtained using crystals prepared by sublimation (Tables 2 and S5; Figure 1B). The hydroxyl hydrogens were located from the difference map and refined. The asymmetric unit contains three TEMPO-H molecules and one water molecule that are hydrogen bonded in a chain. The d(N−O) in TEMPO-H (1.46 ± 0.06 Å) is substantially longer than that in TEMPO (1.283(9) Å)[31] because the radical has a partial N−O π bond.

II. Kinetics and Thermodynamics. A. $Fe^{II}(H_2bip)$ + TEMPO. The reaction between **$Fe^{II}(H_2bip)$** and TEMPO (eq 5) is close to isoergic in MeCN at 298 K ($\Delta G° = -0.3 \pm 0.2$ kcal mol^{-1}), which allows both the forward (k_5) and reverse (k_{-5}) rate constants to be measured directly. Kinetics have been measured in both directions by stopped-flow rapid-scanning UV−vis spectrophotometry under pseudo-first-order conditions. In the forward direction with excess TEMPO, the disappearance of **$Fe^{II}(H_2bip)$** (λ_{max} = 510 nm) and concomitant growth of **$Fe^{III}(Hbip)$** (λ_{max} = 636 nm) was observed (Figure 2A). The spectra were fit over the entire wavelength region observed (a 225 nm window) using the OLIS SVD global analysis software;[32] the match at one wavelength is shown in Figure 2B. The data follow a first-order kinetic model for >4 half-lives. The derived pseudo-first-order rate constants vary linearly with [TEMPO] up to 0.16 M (1600 equiv) and are independent of the initial concentration of **$Fe^{II}(H_2bip)$** from 0.10 to 0.28 mM, Figure S1. These data imply a simple second-order kinetic rate law $R = k_5$[**$Fe^{II}(H_2bip)$**][TEMPO] with $k_5 = 260 \pm 30$ M^{-1} s^{-1} at 298 K (all rate and equilibrium constants and thermochemical values in this report are in MeCN unless otherwise indicated). For the reverse direction, **$Fe^{III}(Hbip)$** + TEMPO-H, the pseudo first-order rate constants are linear with [TEMPO-H] up to 0.05 M (but not above this concentration, see later in this paper). The derived second-order rate constant k_{-5} is 150 ± 20 M^{-1} s^{-1} (Figures S1 and S2).

The rate constants k_5 and k_{-5} were measured over the temperature range of 277−328 K. Remarkably, k_5 shows a small but definite decrease as the temperature increases. Eyring analysis gives $\Delta H_5^{\ddagger} = -2.7 \pm 0.4$ kcal mol^{-1}, $\Delta S_5^{\ddagger} = -57 \pm 8$ cal mol^{-1} K^{-1}, $\Delta H_{-5}^{\ddagger} = 6.7 \pm 0.4$ kcal mol^{-1}, and $\Delta S_{-5}^{\ddagger} = -26 \pm 2$ cal mol^{-1} K^{-1}. The ratio of k_5/k_{-5} is the equilibrium constant K_5 (Figure 3, blue circles). At 298 K, $K_5 = 1.7 \pm 0.3$, close to one, but it is highly temperature dependent. van't Hoff analysis yields $\Delta H°_5 = -9.4 \pm 0.6$ kcal mol^{-1} and $\Delta S°_5 = -30 \pm 2$ cal mol^{-1} K^{-1}. These are unusually large ground-state entropy values for HAT reactions. All errors are reported as $\pm 2\sigma$ based on fits weighted with the errors propagated from experimental measurements (see Experimental Section).

K_5 was independently measured using static UV−vis experiments. Kinetically equilibrated mixtures of **$Fe^{II}(H_2bip)$** and TEMPO in MeCN were perturbed with aliquots of TEMPO and TEMPO-H (Figure S3). After each perturbation, the optical spectrum was deconvoluted into its component absorbances of **$Fe^{III}(Hbip)$**, **$Fe^{II}(H_2bip)$**, and TEMPO (TEMPO-H has no significant absorbance in this spectral region). The resulting equilibrium constants determined over a range of conditions were then averaged to give a single value (see Experimental Section and Table S1). Over a range of temperatures (285−322 K), these static measurements closely match the values obtained from the kinetic data; at 298 K, K_5 (static) = 1.9 ± 0.3 versus K_5 (kinetic) = 1.7 ± 0.3. Figure 3 shows this close agreement between static (blue diamonds) and kinetic (blue circles) data. These two independent measures of the equilibrium constant give the same ground-state enthalpy and entropy changes within error, confirming the large ground-state entropy associated with this reaction (Table 3).

B. $Fe^{II}(H_2bim)$ + TEMPO. Stopped-flow kinetics for the thermodynamically downhill reaction of **$Fe^{III}(Hbim)$** + TEMPO-H, the reverse of reaction 6 (k_{-6}), have been previously described,[33] including the temperature dependence and activation parameters (Table 3). The rate constant for the uphill reaction, k_6, has been determined by stopped-flow UV−vis spectrophotometry using a second-order approach to equilibrium conditions with a large excess of TEMPO (1000−7000 equiv). Global analyses of the spectra with SPECFIT,[34] over the entire

(30) Ozinskas, A. J.; Bobst, A. M. *Helv. Chim. Acta* **1980**, *63*, 1407−1411.
(31) Capiomont, P. A.; Lajzerowicz-Bonneteau, J. *Acta Crystallogr., Sect. B* **1974**, *30*, 2160−2166.
(32) Matheson, I. B. C. *RSM-1000 Global Fit Software*, version 6.3.8; On-Line Instrument Systems (Olis), Inc.: Bogart, GA, 1998.
(33) Roth, J. P. Intrinsic and Thermodynamic Influences on Hydrogen Atom Transfer Reactions Involving Transition Metal Complexes. Ph.D. Thesis, University of Washington, Seattle, WA, 2000.
(34) SPECFIT/32, versions v3.0.26 and v3.0.36; Spectrum Software Associates: Marlbourough, MA, 2000.

Table 2. Selected Bond and Hydrogen Bond Distances (Å) and Angles (deg) for TEMPO-H·$^1/_3H_2O$

Bond Distances and Angles[a]		Hydrogen Bond Distances and Angles				
		D–H···A	*d*(D–H)	*d*(H···A)	*d*(D···A)	∠(DHA)
N(1)−O(1)	1.456 ± 0.06	O(2)−H(2)···O(1)	0.89(2)	1.94(2)	2.830(2)	175(2)
∠O(1)−N(1)−C(1)	107.02 ± 0.02	O(1)−H(1)···O(3)	0.88(2)	2.00(2)	2.882(2)	173(2)
∠O(1)−N(1)−C(5)	106.9 ± 0.1	O(3)−H(3)···O(4)	0.83(3)	1.86(2)	2.685(2)	158(3)
∠C(1)−N(1)−C(5)	119.2 ± 0.9					

[a] Averages and range for the three unique molecules in the unit cell; numbering given for molecule 1.

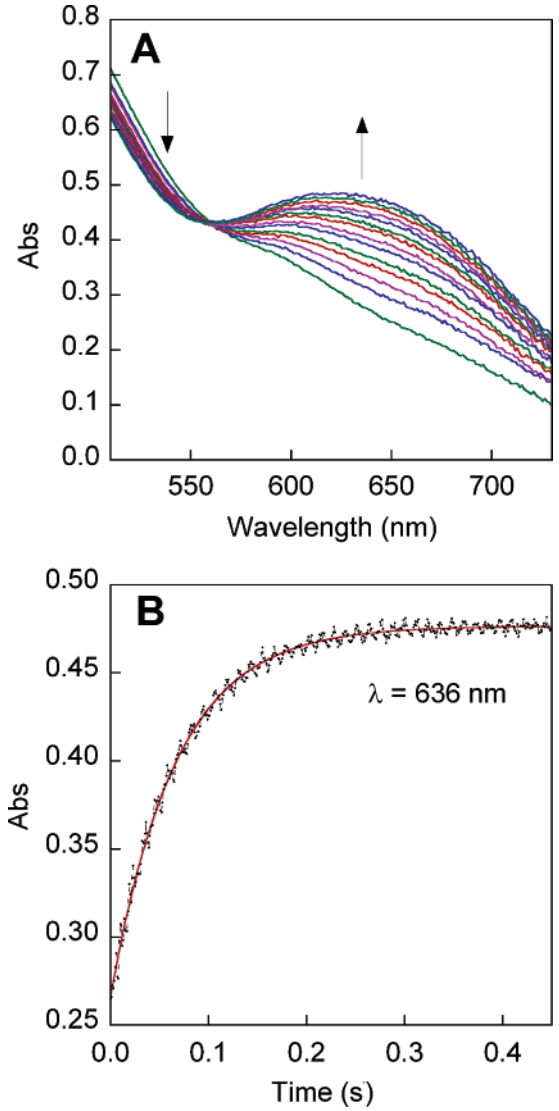

Figure 2. (A) Time evolution of UV-visible spectra of 0.1 mM **$Fe^{II}(H_2$bip)** + 6 mM TEMPO (eq 6) over 0.5 s at 298 K in MeCN. (B) Match between the original data (●) and the pseudo-first-order fit (red −) resulting from OLIS SVD Global Analysis over the whole wavelength region in A (shown only for a single wavelength, 636 nm).

wavelength range collected and using the values of k_{-6} measured, gave the second-order rate constants, k_6. The derived second-order rate constants are independent of the concentration of TEMPO up to 0.46 M (7000 equiv), as shown in the Supporting Information, together with typical spectral traces and a kinetic fit (Figures S4−S7). At 298 K, $k_6 = 0.62 \pm 0.08$ M^{-1} s^{-1}; $k_{-6} = (3.1 \pm 0.1) \times 10^3$ M^{-1} s^{-1}. Eyring plots of rate constants from 288 to 338 K (Figure 4) give the activation parameters in Table 3.

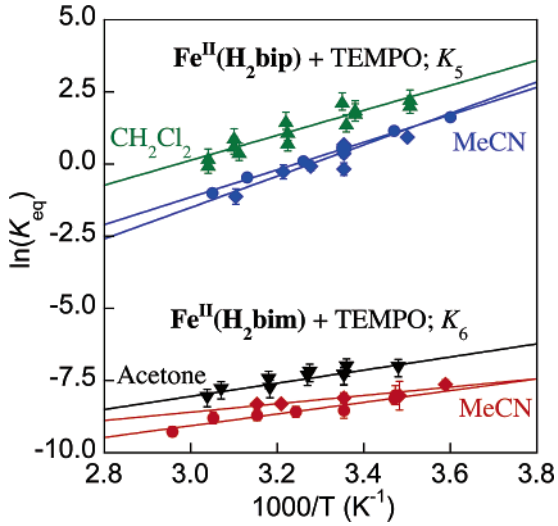

Figure 3. van't Hoff plots. Top: **$Fe^{II}(H_2$bip)** + TEMPO (eq 5); kinetic measurements in MeCN (blue ●); static measurements in MeCN (blue ♦); static measurements in CH_2Cl_2 (green ▼). Bottom: **$Fe^{II}(H_2$bim)** + TEMPO (eq 6); kinetic measurements in MeCN (red ●); static measurements in MeCN (red ♦); static measurements in acetone (black ▼).

As in the **$Fe^{II}(H_2$bip)** case described previously in this paper, the equilibrium constant K_6 is given by k_6/k_{-6} and is highly temperature dependent; $\Delta H°_6 = -4.1 \pm 0.9$ kcal mol^{-1}, $\Delta S°_6 = -30 \pm 3$ cal mol^{-1} K^{-1}. These parameters were independently determined using static UV−vis experiments (278−317 K) employing a method similar to that described in the preceding section but accounting for the fact that K_6 favors reactants much more strongly than K_5. The values agree with those from the kinetic measurements quite well; at 298 K, K_6 (static) = $(3.0 \pm 0.5) \times 10^{-4}$ versus K_6 (kinetic) = $(2.0 \pm 0.3) \times 10^{-4}$. The van't Hoff plots (shown in red at the bottom of Figure 3) show that the static and kinetic data yield the same ground-state enthalpy and entropy values, within error, Table 4.

C. Further Studies of the Molecularity of the Equilibria. The equilibrium constants K_5 and K_6 are ratios of opposing second-order rate constants, as described earlier in this paper, and are, therefore, unitless (eq 7, $H_2L = H_2$bip ($i = 5$) or H_2-bim ($i = 6$)). The reactions of **$Fe^{II}(H_2L)$** are first order in

$$K_i = \frac{k_i}{k_{-i}} = \frac{[\mathbf{Fe^{III}(HL)}][\text{TEMPO-H}]}{[\mathbf{Fe^{II}(H_2L)}][\text{TEMPO}]} \qquad (7)$$

[TEMPO] over all accessible concentrations. However, the reactions of **Fe^{III}(HL)** show saturation behavior at high [TEMPO-H], with **Fe^{III}(Hbip)** at [TEMPO-H] > 0.2 M and with **Fe^{III}(Hbim)** at [TEMPO-H] > 0.01 M. Such saturation behavior is common for reactions which have a rapid pre-

Table 3. Rate Constants and Activation Parameters for Reactions 5 and 6 (MeCN, 298 K)

HX + Y		k ($M^{-1}s^{-1}$)	$\Delta H^{\ddagger a}$	$\Delta S^{\ddagger b}$	K_{eq}
$Fe^{II}(H_2bip)$ + TEMPO	k_5	260 ± 30	−2.7 ± 0.4	−57 ± 8	1.7 ± 0.3
	k_{-5}	150 ± 20	6.7 ± 0.4	−26 ± 2	
$Fe^{II}(H_2bim)$ + TEMPO	k_6	0.62 ± 0.08	4.1 ± 0.3	−45 ± 2	$(2.0 \pm 0.3) \times 10^{-4}$
	k_{-6}[c]	$(3.1 \pm 0.1) \times 10^3$	7.7 ± 0.6	−16 ± 1	

[a] Units: kcal mol^{-1}. [b] Units: cal mol^{-1} K^{-1}. [c] Values for k_{-6} from reference 33.

equilibrium step[35] and suggests that a hydrogen-bonded adduct dominates at high concentrations (e.g., eq 8).

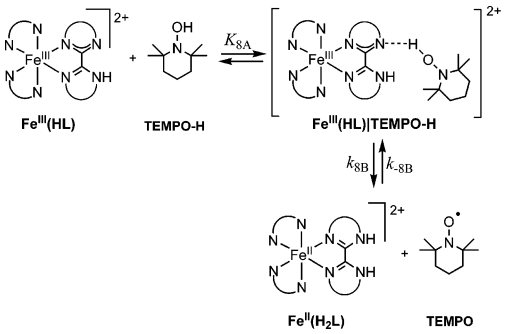

(8)

$$k_{obs} = \frac{K_{8A}k_{8B}[\text{TEMPO-H}]}{1 + K_{8A}[\text{TEMPO-H}]} \quad (9)$$

Fitting the **Fe^{III}(Hbip)** kinetics to the saturation rate law (eq 9, derived for conditions of high [TEMPO-H] where k_{-8B} is negligible) gives values for the pre-equilibrium of $K_{8A} = 3.1 \pm 0.3$ M^{-1} and $k_{8B} = 59 \pm 6$ s^{-1}. Consistent with this analysis, the product $K_{8A}k_{8B}$ (=183 ± 20 M^{-1} s^{-1}) is equal within error to the value of k_{-5} measured at lower [TEMPO-H], 150 ± 20 M^{-1} s^{-1}. For **Fe^{III}(Hbim)** + TEMPO-H, the pre-equilibrium values are $K_{8A} = 56.6 \pm 1.7$ M^{-1} and $k_{8B} = 57.4 \pm 1.8$ s^{-1} (Figure S8; $K_{8A}k_{8B} = 3250 \pm 40$ M^{-1} s^{-1}; $k_{-6} = 3100 \pm 100$ M^{-1} s^{-1}).

It should be emphasized that this saturation is seen only well above the experimental conditions used to determine the unitless K_5 and K_6, from which the thermochemical data are derived (cf. Figure 3). The hydrogen-bonded adducts are not present in significant concentrations under typical measurement conditions. As further confirmation, we note that the optical spectrum of **Fe^{III}(Hbip)** appears to be sensitive to the hydrogen-bonding environment, as the λ_{max} shifts from 636 to 610 nm upon addition of MeOH to 1.17 M ([**Fe^{III}(Hbip)**] = 86 μM). This spectral shift is not observed for **Fe^{III}(Hbip)** at [TEMPO-H] up to ~0.12 M, although such a shift is observed when [TEMPO-H] ≥ 0.4 M. Solutions of pure **Fe^{III}(Hbip)** and **Fe^{III}(Hbim)** follow Beer's Law over the accessible concentration and wavelength ranges (0.06 − 0.8 mM, 400−750 nm), indicating that the iron complexes do not cluster in solution.

As additional confirmation of the unitless nature of the equilibrium constants (eq 7), the static equilibrium mixtures of reactions 5 and 6 have been diluted with MeCN. No variation in the ratio of **$Fe^{II}(H_2L)$/Fe^{III}(HL)** is observed, within error, over a 40% change in volume (Figure 5). The red, dashed line in Figure 5 shows the dependence predicted for a concentration-dependent equilibrium constant, as would be observed, for instance, if K_{8A} was very large (i.e., if all of the **Fe^{III}(HL)** was complexed) and if what was measured was $K_{8B} = k_{8B}/k_{-8B}$. The blue, horizontal line shows the prediction for a unitless equilibrium constant (eq 7).

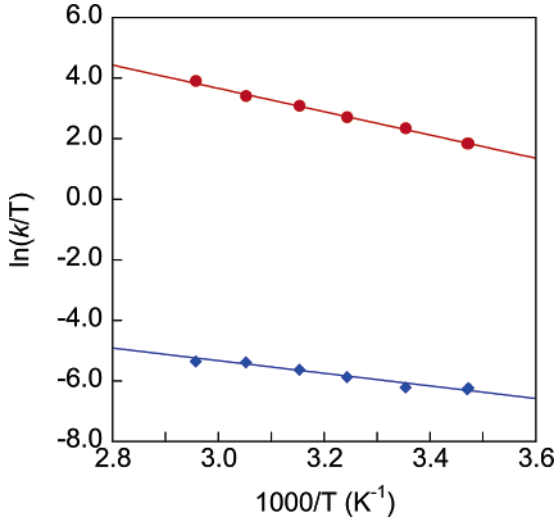

Figure 4. Eyring plots for **$Fe^{II}(H_2bim)$** + TEMPO (k_6; blue ♦) and **Fe^{III}(Hbim)** + TEMPO-H (k_{-6}; red ●) in MeCN.

The equilibrium constant K_5 in acetonitrile is unaffected by the addition of tetrabutylammonium perchlorate ($^nBu_4NClO_4$) up to 0.17 M. This represents a change in ionic strength of approximately 3 orders of magnitude ($I = 1.8 \times 10^{-4} - 0.17$ M; Figure S9). The lack of an ionic strength dependence shows that there is no difference between the ion pairing of the reactants versus that of the products. This further indicates that eqs 5 and 6 are simple opposing bimolecular reactions with unitless equilibrium constants.

D. Solvent Effects. Equilibrium constants have been determined in CH_2Cl_2 for **$Fe^{II}(H_2bip)$** + TEMPO (eq 5) and in acetone for **$Fe^{II}(H_2bim)$** + TEMPO (eq 6). A wider range of solvents is precluded by the solubility and reactivity of the dicationic iron species. These experiments used the static equilibrium method described previously in this paper for MeCN, yielding $K_{5CH_2Cl_2} = 5.4 \pm 0.7$ and $K_{6Me_2CO} = (6.7 \pm 0.2) \times 10^{-4}$ (both at 298 K). There is very little change in the absorption spectra of TEMPO, **$Fe^{II}(H_2L)$**, and **Fe^{III}(HL)** as a function of solvent,[36] and the equilibrium mixtures qualitatively appear very similar to those in MeCN. Quantitatively, $K_{5CH_2Cl_2}$ and K_{6Me_2CO} are each approximately three times larger than the K's in MeCN at 298 K. The temperature dependences of these equilibria give $\Delta H°$ and $\Delta S°$ values that are within error of those determined in MeCN, as summarized in Table 4 and shown in

(35) Espenson, J. H. *Chemical Kinetics and Reaction Mechanisms*, 2nd ed. McGraw-Hill, Inc.: New York, 1995, pp 70−95 and p 158.

(36) The solvatochromism for TEMPO is negligible in our measurements in MeCN, CH_2Cl_2, and acetone but is significant in a wider range of solvents: Glowacka, J.; Szczepek, W. J.; Wrona, P. K. *Pol. J. Chem.* **2000**, *74*, 1341−1348.

Table 4. Equilibrium Constants and Ground-State Thermodynamics for Hydrogen Atom and Electron-Transfer Reactions in Different Solvents

HX + Y	solvent	method	K_{eq} (298 K)	$\Delta H°$ (kcal mol^{-1})	$\Delta S°$ (cal mol^{-1} K^{-1})
Fe^{II}(H$_2$bip) + TEMPO	MeCN	kinetic	1.7 ± 0.3	-9.4 ± 0.6	-30 ± 2
	MeCN	static	1.9 ± 0.3	-8.7 ± 0.8	-28 ± 3
	CH_2Cl_2	static	5.4 ± 0.7	-8.6 ± 0.9	-25 ± 5
Fe^{II}(H$_2$bim) + TEMPO	MeCN	kinetic	$(2.0 \pm 0.3) \times 10^{-4}$	-4.1 ± 0.8	-30 ± 2
	MeCN	static	$(3.0 \pm 0.5) \times 10^{-4}$	-3.1 ± 0.9	-27 ± 3
	Acetone	static	$(7 \pm 1) \times 10^{-4}$	-4.5 ± 0.7	-30 ± 2
Fe^{II}(H$_2$bim) + [CpCp*Fe]$^+$	MeCN	static	5.5 ± 0.8	-6.0 ± 0.9	-17 ± 3

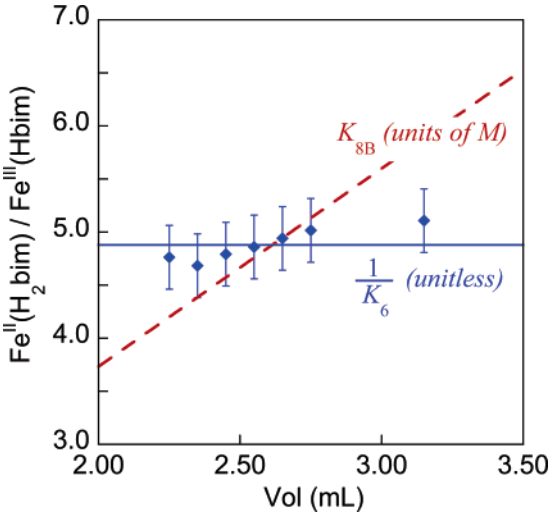

Figure 5. Plot of **Fe^{II}(H$_2$bim)/Fe^{III}(Hbim)** versus total volume upon dilution of an equilibrium mixture of 1.03 μmol of **Fe^{II}(H$_2$bim)** and 85.5 μmol of TEMPO (eq 6) with MeCN. The blue horizontal line (—) is the prediction for the unitless $1/K_6$ (eq 7). The red dashed line (- - -) is the prediction for an equilibrium constant with units of M, for instance, involving a hydrogen-bonded adduct such as K_{8B} ($=k_{8B}/k_{-8B}$) in eq 8.

the van't Hoff plots in Figure 3 (K_5 in CH_2Cl_2 in green, K_6 in acetone in black). Thus, solvation and hydrogen bonding to solvent cannot fully account for the observed entropy effects in these reactions. The $\Delta S°$ varies slightly with solvent but still remains large and negative in all cases.

III. Comparison with an Electron-Transfer Reaction. The electron-transfer (ET) reaction between **Fe^{III}(H$_2$bim)** and 1,2,3,4,5-pentamethylferrocene (CpCp*Fe) (eq 10) has been studied in MeCN in order to compare the entropy changes for

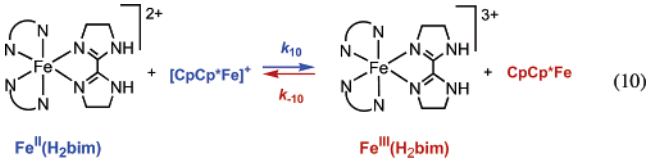

(10)

ET versus HAT. Addition of 0−0.3 equiv of CpCp*Fe to a 2 mM solution of **Fe^{III}(H$_2$bim)** yields **Fe^{II}(H$_2$bim)** and the distinctive [CpCp*Fe]$^+$ ion (λ_{max} = 740 nm, ϵ = 353 M^{-1} cm^{-1}).[37] The conversion is not quantitative, and equilibrium is established between the four species present (Figure 6A). The large excess of **Fe^{III}(H$_2$bim)** prevents direct

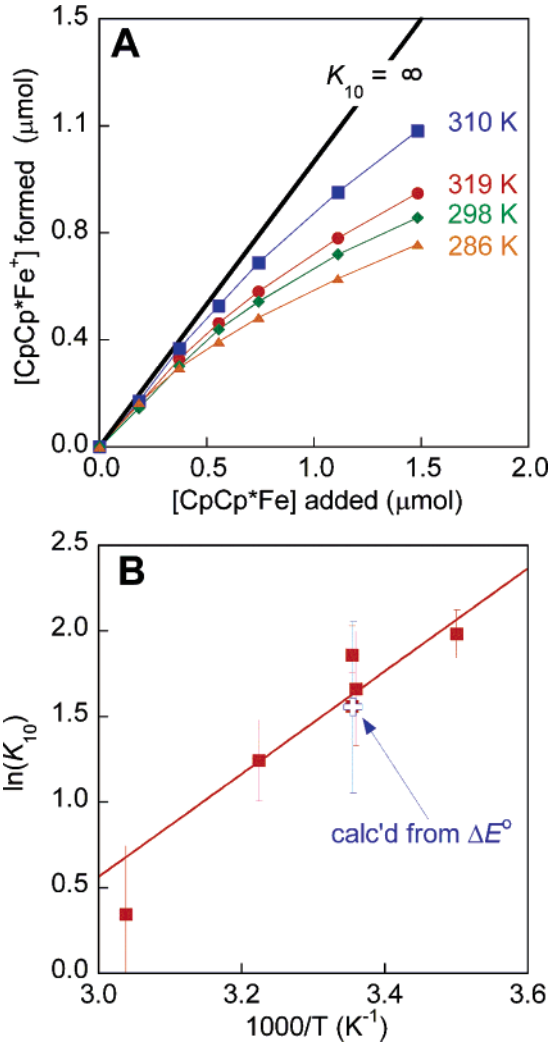

Figure 6. **Fe^{II}(H$_2$bim)** + [CpCp*Fe]$^+$ (eq 10; MeCN, 0.09 M ^{n}Bu$_4$NClO$_4$). (A) Formation of [CpCp*Fe]$^+$ as a function of added CpCp*Fe at various temperatures. (B) van't Hoff plot.

quantification of all but [CpCp*Fe]$^+$ by optical spectroscopy; however, based on the starting conditions, the equilibrium constant for the process can be extracted (analogous to the analysis for eq 6) as K_{10} (298 K) = 5.5 ± 0.8 (Figure S10). This is in good agreement with the equilibrium constant of ~5 predicted from the difference in redox potentials ($E_{1/2}$(**Fe^{III}(H$_2$bim)**) = −0.31 ± 0.05 V;[27] $E°$([CpCp*Fe][ClO$_4$]) = −0.272 ± 0.003 V;[38] lnK_{10} = 1.6 ± 1.9).[39] All ET reactions were done at a constant ionic strength, 0.09 M ^{n}Bu$_4$NClO$_4$. The

(37) Our measurements of the [CpCp*Fe]$^+$ λ_{max} and ϵ are close to previous reports: (a) Nelsen, S. F.; Chen, L.-J.; Ramm, M. T.; Voy, G. T.; Powell, D. R.; Accola, M. A.; Seehafer, T. R.; Sabelko, J. J.; Pladziewicz, J. R. *J. Org. Chem.* **1996**, *61*, 1405−1412. (b) Nelsen, S. F.; Wang, Y.; Ramm, M. T.; Accola, M. A.; Pladziewicz, J. R. *J. Phys. Chem.* **1992**, *96*, 10654−10658. (c) Duggan, D. M.; Hendrickson, D. N. *Inorg. Chem.* **1975**, *14*, 955−970.

(38) Noviandri, I.; Brown, K. N.; Fleming, D. S.; Gulyas, P. T.; Lay, P. A.; Masters, A. F.; Phillips, L. *J. Phys. Chem. B* **1999**, *103*, 6713−6722.

(39) All potentials are referenced in MeCN with 0.1 M NBu$_4$ClO$_4$ versus ferrocene.

Scheme 1. Entropy of Electron Transfer: **$Fe^{III}(H_2bim)$** + CpCp*Fe

	ΔS° (cal mol^{-1} K^{-1})
$[Fe^{II}(H_2bim)_3]^{2+} + [CpCp^*Fe]^{+} \longrightarrow [Fe^{III}(H_2bim)_3]^{3+} + CpCp^*Fe$	-17 ± 3
$CpCp^*Fe \longrightarrow [CpCp^*Fe]^{+} + e^-$	-11.7 ± 0.5
$[Fe^{II}(H_2bim)_3]^{2+} \longrightarrow [Fe^{III}(H_2bim)_3]^{3+} + e^-$	-29 ± 3

equilibrium is temperature dependent, and van't Hoff analysis (285−329 K) yields $\Delta H^\circ_{10} = -6.0 \pm 0.9$ kcal mol^{-1} and $\Delta S^\circ_{10} = -17 \pm 3$ cal mol^{-1} K^{-1} (Figure 6).

The overall entropy change for this outer-sphere electron-transfer reaction (ΔS°_{10}) can be described in terms of the component half-reaction entropies $\Delta S^\circ_{CpCp^*Fe}$ and $\Delta S^\circ_{Fe(H_2bim)/ET}$ (eq 11).[40] For $CpCp^*Fe^{+/0}$, $\Delta S^\circ_{CpCp^*Fe} = 11.7 \pm 0.5$ cal mol^{-1} K^{-1} (0.1 M ^{n}Bu$_4$NClO$_4$ in MeCN), as determined by Noviandri and co-workers using the temperature

$$\Delta S^\circ_{10} = \Delta S^\circ_{CpCp^*Fe} - \Delta S^\circ_{Fe(H_2bim)/ET} \qquad (11)$$

dependence of the formal potential.[38] This, in combination with our measurement of ΔS°_{10}, yields $\Delta S^\circ_{Fe(H_2bim)/ET} = 29 \pm 3$ cal mol^{-1} K^{-1} (Scheme 1). This is both the same sign and magnitude as the HAT reaction entropies found previously in this paper (note that, by convention, the ET half-reaction is written as a reduction, opposite to the iron redox couples in eqs 5 and 6).

IV. Calculations. Computations have been performed on a version of reaction 6 where two of the iron ligands have been simplified to 1,4-diazabutadiene and where TEMPO-H has been reduced to NH_2OH (eq 12). The reactants and products were treated as gas-phase hydrogen-bonded adducts. The product has

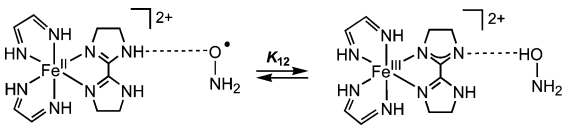

(12)

a dicationic **Fe^{III}(Hbim)** moiety with a spin of $^5/_2$, which is hydrogen-bonded to the zero-charge and -spin $HONH_2$ molecule. The reactant is a **$Fe^{II}(H_2bim)$** unit with the same 2+ charge and a nominal spin of 2 (high-spin d^6), coupled to a neutral, spin $^1/_2$, $^\bullet ONH_2$ radical. Ferromagnetic coupling has been assumed, both for ease of computation and to give a spin-allowed reaction, so that the reactant has an overall spin of $^5/_2$. In this model, the reaction is a simple hydrogen transfer, N−H···$^\bullet$O ⇆ N$^\bullet$···H−O, with concomitant structural reorganization of the reagents.

Initial calculations using the B3LYP functionals in DFT with a 6-31G* basis set failed to reproduce the observed ground state for **Fe^{III}(Hbim)**. Instead, these predicted a d^6, $S = 2$ Fe^{II} center coupled to an Hbim radical, with spin $^1/_2$ on the deprotonated ring. Considering only the active N═C−N̈H part of the ligand, the calculations show a π-allyl-type radical, N═C−Ṅ: ↔ Ṅ−C═N:. That is, H^+ was apparently removed from the N σ lone pair, but the e^- was removed from the π system. This model calculation gave a predicted entropy decrease of only 5 cal K^{-1} mol^{-1}, which was associated mostly with changes in vibrational frequencies.

Ordinarily, DFT results are more reliable than UHF results for transition-metal complexes. In view of the failure of DFT, however, we resorted to a UHF calculation with the same basis set. This gave a wave function in qualitative agreement with the experimental conclusions. The Fe center in the reactant had a Mulliken population of 4.0 net spin-up electrons and a total charge of 1.6, in agreement with the d^6, $S = 2$ Fe^{II} label. The product Fe center was computed to have 4.7 net spin-up electrons and a total charge of 2.1, in fair agreement with a d^5, $S = ^5/_2$ Fe^{III} description. There was a small 0.2 net spin-up on the Hbim group and a change in its net charge of −0.6 electrons. Thus, this model predicts a coupled (e^-, H^+) transfer of a proton from the H_2bim and an electron from the Fe center.

Associated with this oxidation of the Fe, deprotonation of H_2bim, and reduction of the $^\bullet ONH_2$, there is a significant change in bond lengths. The Fe−N distance in the ring from which the H is removed shortens by 0.27 Å, and all of the other Fe−N distances shorten by 0.16−0.08 Å. These are in the same direction but somewhat larger than the differences between the solid-state structures of high-spin **$Fe^{II}(H_2bim)$** and high-spin **Fe^{III}(Hbim)**; Δd(Fe−N) = 0.17 Å for the deprotonating ring and an average of 0.07 Å for the others (Table 1).[27] In the active N═C−N̈H part of H_2bim, the N═C double bond is calculated to lengthen from 1.28 to 1.37 Å (1.27 to 1.33 Å in the solid-state structures), while the N−C single bond shortens from 1.33 to 1.26 Å when the (e^-, H^+) pair is removed (1.34−1.31 Å in the solids). These bond length differences lead to extensive changes in many of the low-frequency vibrational modes.

These changes in bonding lead to a predicted entropy decrease, $\Delta S^\circ_{12} = -18.7$ cal mol^{-1} K^{-1}. The calculation is done with constant spin and mass; therefore, this entropy can only come from rotational and vibrational sources. The calculation shows that the contribution from the change in moment of inertia is small, as would be expected from a reaction in which the primary chemical change is the ∼1 Å movement of a hydrogen atom. Changes in vibrational frequencies account for 18.4 cal mol^{-1} K^{-1} of the ΔS° in this system. This is spread over the 30 or so modes with frequencies $h\nu$ on the order of kT (207 cm^{-1} at 298 K). These are bending and torsional vibrations, not stretches (which are at much higher frequency), where each mode contributes between 0.5 and 6 cal mol^{-1} K^{-1} to the total entropy. Calculated vibrational frequencies and their entropic contributions are given in Tables S2 and S3. It should be noted that this calculation neglects possible electronic contributions to the entropy, although these are expected to be small. If the reactant pair is antiferromagnetically coupled to give a total spin of $S = ^3/_2$ (which would make the overall reaction forming $S = ^5/_2$, high-spin Fe^{III} spin-forbidden), there would be a spin contribution to the entropy of +0.8 cal mol^{-1} K^{-1} ($T\Delta S = 0.2$ kcal mol^{-1} at 298 K).[41] There could also be a small entropy contribution from low-lying electronic states of the high-spin d^6 configuration.

(40) (a) Yee, E. L.; Cave, R. J.; Guyer, K. L.; Tyma, P. D.; Weaver, M. J. *J. Am. Chem. Soc.* **1979**, *101*, 1131−1137.

(41) For system with spin S, the number of states $W = 2S + 1$ and the spin entropy $S^\circ = R\ln(W)$. For a spin change from $^3/_2$ to $^5/_2$, $\Delta S^\circ = R\ln(2[^5/_2] + 1) - R\ln(2[^3/_2] + 1) = 0.8$ cal mol^{-1} K^{-1}.

(42) NIST Chemistry WebBook. NIST Standard Reference Database Number 69. http://webbook.nist.gov/chemistry/ (March 2003 release).

(43) Burcat, A.; Ruscic, B. TAE Report No. 960. Technion: Haifa, Israel, 2005; see also ftp://ftp.technion.ac.il/pub/supported/aetdd/thermodynamics.

(44) Ruscic, B.; Boggs, J. E.; Burcat, A.; Császár, A. G.; Demaison, J.; Janoschek, R.; Martin, J. M. L.; Morton, M. L.; Rossi, M. J.; Stanton, J. F.; Szalay, P. G.; Westmoreland, P. R.; Zabel, F.; Bérces, T. *J. Phys. Chem. Ref. Data* **2005**, *34*, 573−656.

(45) Curran, H.; Wu, C.; Marinov, N.; Pitz, W. J.; Westbrook, C. K.; Burcat, A. *J. Phys. Chem. Ref. Data* **2000**, *29*, 463−517.

Table 5. Gas-Phase Entropy Differences for HAT Couples AH versus A•[a]

AH/A•	$S°(AH)_g$[a]	$S°(A•)_g$[a]	$\Delta S° = S°(A•)_g - S°(AH)_g$
HCl/Cl•	44.67[b]	39.48[b]	−5.19
H_2O/•OH	45.13[c]	43.90[d]	−1.23
NH_3/•NH_2	46.07[c]	46.57[d]	0.50
CH_4/•CH_3	44.54[c]	46.37[d]	1.83
CH_3OH/CH_3O•	57.32[c]	55.99[d]	−1.33
C_6H_5OH/C_6H_5O•	75.34[c]	74.54[c]	−0.80
C_6H_6/•C_6H_5	64.33[c]	68.37[c]	4.04
toluene/benzyl radical	76.53[c]	76.06[d]	−0.47
pyridine/3-pyridyl radical	67.58[c]	69.84[c]	2.26
naphthalene/1-naphthyl radical	79.89[e]	84.36[e]	4.47

[a] Data in cal mol^{-1} K^{-1} at 298.15 K unless otherwise noted. [b] Reference 42. [c] Reference 43. [d] Reference 44. [e] Reference 45; values at 300 K.

Discussion

I. Overview of Hydrogen Atom Transfer Entropies. A hydrogen atom transfer reaction (eq 13) can be considered as the sum of two half-reactions (e.g., eq 14), analogous to electron-transfer processes. The half-reaction is the definition of the bond

$$A{-}H + B^{\bullet} \rightarrow A^{\bullet} + H{-}B \qquad \Delta G°_{13}, \Delta H°_{13}, \Delta S°_{13} \quad (13)$$

$$A{-}H \rightarrow A^{\bullet} + H^{\bullet} \qquad \text{BDFE, BDE} \quad (14)$$

dissociation free energy (BDFE) and bond dissociation enthalpy (BDE). The general assumption that the entropies of AH and A• are very similar (eq 15) has the corollary that, for HAT

$$S°(AH) \approx S°(A^{\bullet}) \quad (15)$$

reactions, the overall entropy change should be small, $\Delta S°_{13} \approx 0$. Equation 15 is an implicit assumption in the widely accepted thermochemical cycles used to derive BDEs from acidity (pK_a) and redox potential ($E_{1/2}$), as discussed later in this paper. Equation 15 will not be strictly accurate because AH and A• have different moments of inertia and different spin states, but these are, in most cases, small effects. For instance, the (molar) entropy resulting from a change from spin 0 to spin $^1/_2$ is $R\ln(2)$ or 1.4 cal mol^{-1} K^{-1} ($T\Delta S° = 0.42$ kcal mol^{-1}). Even for organic systems in which free or slightly hindered rotations in AH become essentially frozen in A•, entropy changes still appear to be small. For the prototypical example of toluene versus benzyl radical, $\Delta S°$ is only −0.47 cal mol^{-1} K^{-1} (Table 5). The entropy data that are available for small organic and main-group species in the gas phase provide support for eq 15. $|S°(A^{\bullet})_g - S°(AH)_g|$ is <5.2 cal mol^{-1} K^{-1} for the various molecules in Table 5. This corresponds to a change in an equilibrium constant of less than a factor of 14, or ≤1.5 kcal mol^{-1} in $\Delta G°$ at 298 K.

For HAT reactions in solution, the entropy changes are small when the analogous gas-phase reaction has $\Delta S°_{13} \approx 0$ and when the entropies of solvation are comparable (eq 16). A few

$$\Delta S°_{solv}[AH] + \Delta S°_{solv}[B^{\bullet}] \approx \Delta S°_{solv}[BH] + \Delta S°_{solv}[A^{\bullet}] \quad (16)$$

entropies for HAT reactions have been reported for organic molecules in solution, which support this assumption, $\Delta S°_{13}$ (solution) ≈ 0. For example, the reaction between galvinoxyl radical and 2,4,6-tri-*tert*-butylphenol is thermodynamically uphill ($\Delta G° = 2.6$ kcal mol^{-1}) in toluene and has $\Delta S° = -0.7 \pm 0.6$ cal mol^{-1} K^{-1}.[46] The related hydrogen atom transfer between the α-tocopherol radical and phenothiazine has $\Delta S° = -1.2 \pm 3.0$ in benzene.[47] There are even fewer examples of related inorganic systems in solution where the ground-state entropy change has been determined. Norton and co-workers have calculated $\Delta S°(AH) - \Delta S°(A^{\bullet}) = -2.68$ cal mol^{-1} K^{-1} for $CpCr(CO)_3H$.[23b] Wayner and Parker used a series of thermochemical cycles to conclude that $\Delta S°_{13} \approx 0$ for a wide range of transition-metal hydrides.[23a,48] In sum, previously published studies of HAT reactions support the common assumption that $\Delta S°_{13}$ is close to zero and, therefore, that $\Delta G°_{HAT} \approx \Delta H°_{HAT} = \Delta BDE$.

II. Origin of the Large Entropy of the $Fe^{II}(H_2L)$ Reactions. The reactions of **$Fe^{II}(H_2bip)$** and **$Fe^{II}(H_2bim)$** with TEMPO contradict the common assumption that entropy changes are not significant in HAT reactions. These reactions have $\Delta S° \approx -30$ cal mol^{-1} K^{-1}, the negative sign indicating that **$Fe^{III}(HL)$** + TEMPO-H is the more ordered side of eqs 5 and 6. A variety of possible origins of this entropy change are considered in the following sections.

A. Translational Entropy: 1. Molecularity. For a bimolecular reaction, −30 cal mol^{-1} K^{-1} would be a typical entropy of activation, $\Delta S^{\ddagger}$.[35] This is due to the loss of translational entropy required to bring two freely diffusing reactants together. A similar value of the ground-state entropy, $\Delta S°$, would be expected for a reaction where two separate reactants combine to form one product. For reactions 5 and 6, however, a number of lines of evidence indicate that there are equal numbers of reactants and products. The reactions obey simple second-order kinetics under the conditions where the $\Delta S°$ is determined, showing saturation kinetics only at high [TEMPO-H]. Similar values for $\Delta S°_5$ and $\Delta S°_6$ are found for both system measurements despite the difference in K_{8A}, 3.1 and 57 M^{-1} for eqs 5 and 6, respectively. If there were a change in the number of molecules during the reaction, the position of equilibrium would be a function of concentration, but no such dependence is observed in static experiments (cf. Figure 5). Thus, a change in translation entropy between the reactants and products is not the origin of the large $|\Delta S°|$.

2. Ion Pairing. The iron reagents in eqs 5 and 6 are charged and, therefore, have counterions that could be ion-paired to different extents under different conditions. A change in the ion pairing between reactants and products could also cause a change in the molecularity of the reactions and, therefore, the reaction entropy. However, there is no ionic strength dependence in MeCN over 4 orders of magnitude in *I*. In addition, the same entropy change, within error, is observed for eq 5 in both MeCN and CH_2Cl_2, although ion pairing is much stronger in the latter solvent.

3. Solvent Effects/Hydrogen Bonding. Different solvation of the reactants and products is another possible source of the observed ground-state entropy change. Nonspecific solvation

(46) Lucarini, M.; Pedulli, G. F.; Cipollone, M. *J. Org. Chem.* **1994**, *59*, 5063−5070.
(47) Lucarini, M.; Pedrielli, P.; Pedulli, G. F.; Valgimigli, D.; Gigmes, D.; Tordo, P. *J. Am. Chem. Soc.* **1999**, *121*, 11546−11553.
(48) Ref 23a actually finds that $\Delta H°_{solvation}[AH{-}A^{\bullet}] + T\Delta S°_{13}[AH{-}A^{\bullet}] \approx -2.2$ kcal mol^{-1} in MeCN, which the authors contribute mostly to $\Delta H°_{solvation}[AH{-}A^{\bullet}]$.

of charged ions involves the organization of polar solvent molecules and has significant entropic effects. In reactions 5 and 6, the iron reactants ($Fe^{II}(H_2L)$) and products ($Fe^{III}(HL)$) have the same 2+ charge and are almost the same size (despite the change in d(Fe−N) of ∼0.1 Å); therefore, their solvation (and ion pairing) should be very similar. In general, for reactions that involve only transfer of a neutral H atom, there are likely to be only very small changes in nonspecific solvation.

There could, however, be significant changes in the interactions of the reactants with particular solvent molecules, for instance, different hydrogen bonding. Reactions of phenols show very large kinetic solvent effects because of the ArO−H··· solvent hydrogen bond, which is not present at the transition state.[49] In the absence of hydrogen-bonding effects, HAT reactions are often insensitive to solvent; the rate constants for cumyloxyl radical plus cyclohexane are the same, within 10%, in CCl_4, C_6H_6, ^{t}BuOH, MeCN, and AcOH.[50] Reactions 5 and 6 are almost this insensitive to solvent. The equilibrium constants increase by only a factor of ∼3 ($\Delta\Delta G° \approx 0.6$ kcal mol^{-1}) upon switching from MeCN to CH_2Cl_2 (for K_5) or from MeCN to acetone (for K_6). The same ground-state entropy changes are observed in all of the solvents, within experimental error (Table 4). MeCN, acetone, and CH_2Cl_2 have quite different polarities (dielectric constants of 37.5, 20.7, and 8.9 respectively[51]); therefore, differential nonspecific solvation is not important to these reactions. Changes in hydrogen bonding are also not significant since CH_2Cl_2 is a much poorer hydrogen-bond acceptor than acetone or MeCN (with $\beta^H_{2(s)}$ values of 0.05, 0.49, and 0.44, respectively in the Abraham scale favored for phenol reactions.)[49,52] None of these solvents is a good hydrogen-bond donor.

In summation, the large magnitude of the entropies for reactions 5 and 6 are not due to translational entropy from different numbers of reactant and product molecules nor is it due to different amounts of ion pairing or solvent effects. Since organic HAT half-reactions have not been observed to have large entropies, the unusual $\Delta S°$ for these reactions is very likely a property of the iron redox couples (the iron HAT half-reactions).

4. Iron Spin Equilibria. In our preliminary report of reaction 5 and its analysis with Marcus Theory, we speculated that the large $|\Delta S°|$ could be due to high-spin/low-spin equilibria for **$Fe^{II}(H_2bip)$** and **Fe^{III}(Hbip)**.[16] Both of these compounds are mixtures of high- and low-spin forms over the accessible temperature range in MeCN solution. **$Fe^{II}(H_2bip)$** in MeCN at 298 K is 88% high-spin and 12% low-spin, and spin interconversion has $\Delta H°_{spin} = -5.1 \pm 0.5$ kcal mol^{-1} and $\Delta S°_{spin} = -21 \pm 2$ cal mol^{-1} K^{-1}.[25] **Fe^{III}(Hbip)** is 16% high-spin and 84% low-spin in MeCN at 298 K, with $\Delta H°_{spin} = -1.9 \pm 0.7$ kcal mol^{-1} and $\Delta S°_{spin} = -3 \pm 2$ cal mol^{-1} K^{-1} (at 298 K).[25] Measurements of reaction 6 were done to test this hypothesis because **$Fe^{II}(H_2bim)$** and **Fe^{III}(Hbim)** are fully high-spin under all of our conditions. The result that the same large entropy change is observed for both the H_2bip and H_2bim systems rules out spin equilibria as the cause of the $\Delta S°$.

5. Vibrational Entropy of the Iron Complexes. While spin equilibria are not the origin of the $\Delta S° \approx -30$ cal mol^{-1} K^{-1} for reactions 5 and 6, it is interesting that there is a similar entropy change for the high-spin to low-spin transition for **$Fe^{II}(H_2bip)$**, −21 cal mol^{-1} K^{-1}.[25] Such large spin-change entropies are common for iron(II) compounds and are due primarily to vibrational entropy ($\Delta S°_{vib}$).[28,54] The solvation and ion-pairing properties are very similar for high- versus low-spin ions, and the electronic contribution to the entropy ($\Delta S°_{elec}$) is small. In the absence of spin−orbit coupling, conversion of a $^5T_{2g}$ state to a $^1A_{1g}$ state has $\Delta S°_{elec} = -5.4$ cal mol^{-1} K^{-1}.[53]

Vibrational entropy ($\Delta S°_{vib}$) has been extensively discussed both for spin equilibria[28,54] and for electron-transfer couples.[55,56] Sorai and Seki were the first to connect changes in metal−ligand vibrations with entropies for spin crossover that were substantially larger than the electronic entropy from the change in spin multiplicities.[57] As illustrated by Richardson and Sharpe (for harmonic vibrations),[55] the major contributors are skeletal vibrations at low energy (≈kT, 207 cm^{-1} at 298 K) that change frequency between reactions and products. Our calculations on eq 12, a model for reaction 6, follow this general pattern. There are approximately 30 vibrations in both the reactant and the product that contribute between 0.5 and 6 cal mol^{-1} K^{-1} to $\Delta S°_{12}$. These are low-frequency (207−330 cm^{-1}) torsion and bending modes. Summing over all of the vibrational modes, the difference between the reactants and products gives $\Delta S°_{12} = -18.4$ cal mol^{-1} K^{-1} from the UHF/6-31G* calculations, reasonable agreement given that the calculations were done at a moderate level of theory (UHF) on a model system in the gas phase. In essence, the Fe^{II} complex is floppier and has more lower frequency modes as compared to those of the Fe^{III} complex.

The **$Fe^{III}(H_2bim) \rightarrow Fe^{II}(H_2bim)$** electron-transfer couple shows a similarly large entropy of $\Delta S°_{Fe(H_2bim)/ET} = 29 \pm 3$ cal mol^{-1} K^{-1}, as determined from the solution ET equilibrium between **$Fe^{III}(H_2bim)$** and CpCp*Fe. This value is the same, within error, as the $\Delta S°$ measured for the overall HAT reactions in eqs 5 and 6 (the sign of $\Delta S°_{Fe(H_2bim)/ET}$ is opposite to that of $\Delta S°_5$ and $\Delta S°_6$ because ET reactions are written as reductions

(49) (a) Snelgrove, D. W.; Lusztyk, J.; Banks, J. T.; Mulder, P.; Ingold, K. U. *J. Am. Chem. Soc.* **2001**, *123*, 469−477. (b) Litwinienko, G.; Ingold, K. U. *J. Org. Chem.* **2005**, *70*, 8982−8990. (c) Litwinienko, G.; Ingold, K. U. *J. Org. Chem.* **2004**, *69*, 5888−5896.

(50) Avila, D. V.; Brown, C. E.; Ingold, K. U.; Lusztyk, J. *J. Am. Chem. Soc.* **1993**, *115*, 466−470.

(51) Riddick, J. A.; Bunger, W. B. Techniques of Chemistry. In *Organic Solvents: Physical Properties and Methods of Purification*, 3rd ed.; Weissberger, A., Ed; Wiley-Interscience: New York, 1970; Vol. 2, pp 243, 349, 400.

(52) (a) Abraham, M. H.; Platts, J. A. *J. Org. Chem.* **2001**, *66*, 3484−3491. (b) Abraham, M. H.; Grellier, P. L.; Prior, D. V.; Taft, R. W.; Morris, J. J.; Taylor, P. J.; Laurence, C.; Berthelot, M.; Doherty, R. M.; Kamlet, M. J.; Abboud, J.-L. M.; Sraidi, K.; Guiheneuf, G. *J. Am. Chem. Soc.* **1988**, *110*, 8534−8536. (c) Abraham, M. H.; Grellier, P. L.; Prior, D. V.; Morris, J. J.; Taylor, P. J. *J. Chem. Soc., Perkin Trans. 2* **1990**, 521−529. (d) Abraham, M. H.; Grellier, P. L.; Prior, D. V.; Duce, P. P.; Morris, J. J.; Taylor, P. J. *J. Chem. Soc., Perkin Trans. 2* **1989**, 699−711.

(53) This is a factor of $^1/_{15}$ in equilibrium constant due to the fifteen-fold degeneracy of the $^5T_{2g}$ state. Any splitting of the states from lower than O_h symmetry or from spin−orbit coupling would reduce $\Delta S°_{elec}$.

(54) (a) Turner, J. W; Schultz, F. A. *Coord. Chem. Rev.* **2001**, *219*−*221*, 81−97. (b) Goodwin, H. A. *Top. Curr. Chem.* **2004**, *233*, 59−90.

(55) (a) Richardson, D. E.; Sharpe, P. *Inorg. Chem.* **1993**, *32*, 1809−1812. (b) Richardson, D. E.; Sharpe, P. *Inorg. Chem.* **1991**, *30*, 1412−1414.

(56) (a) Turner, J. W.; Schultz, F. A. *J. Phys. Chem. B* **2002**, *106*, 2009−2017. (b) Turner, J. W.; Schultz, F. A. *Inorg. Chem.* **2001**, *40*, 5296−5298. (c) Sharpe, P.; Kebarle, P. *J. Am. Chem. Soc.* **1993**, *115*, 782−789. (d) Kratochvil, B.; Knoeck, J. *J. Phys. Chem.* **1966**, *70*, 944−946. (e) Turner, J. W.; Schultz, F. A. *Inorg. Chem.* **1999**, *38*, 358−364. (f) Hupp, J. T.; Weaver, M. J. *Inorg. Chem.* **1983**, *22*, 2557−2564. (g) Sahami, S.; Weaver, M. J. *J. Electroanal. Chem. Interfacial Electrochem.* **1981**, *122*, 155−170. (h) Sahami, S.; Weaver, M. J. *J. Electroanal. Chem. Interfacial Electrochem.* **1981**, *122*, 171−181. (i) Hupp, J. T.; Weaver, M. J. *Inorg. Chem.* **1984**, *23*, 3639−3644. (j) Hupp, J. T.; Weaver, M. J. *Inorg. Chem.* **1984**, *23*, 256−258. (k) Yee, E. L.; Weaver, M. J. *Inorg. Chem.* **1980**, *19*, 1077−1079.

(57) (a) Sorai, M.; Seki, S. *J. Phys. Chem. Solids* **1974**, *35*, 555−570. (b) Tuchagues, J.-P.; Bousseksou, A.; Molnar, G.; McGarvey, J. J.; Varret, F. *Top. Curr. Chem.* **2004**, *235*, 85−103.

by convention). The close numerical agreement between HAT and ET entropies is, in part, fortuitous since the ET reaction involves changes in overall charge and, therefore, solvation. Electron-transfer half-reaction entropies for Fe^{III}/Fe^{II} redox couples are typically found to be 15−30 cal mol^{-1} K^{-1} in organic solvents (excepting those with an accompanying spin change).[55,56] For example, $\Delta S°_{ET}$ for low-spin $[Fe\{B(pz)_4\}_2]^{+/0}$ is 19 ± 1 cal mol^{-1} K^{-1} in MeCN ($[B(pz)_4]^-$ = tetrakis(pyrazol-1-yl)borate).[56a] As emphasized for $[M(OH_2)_6]^{3+/2+}$ ions in aqueous solution, hydrogen bonding can increase half-reaction entropies, but for larger cations in organic solvents, the differences in solvation are small, and $\Delta S°_{ET}$ is dominated by $\Delta S°_{vib}$.[55] While these electron-transfer reactions are not directly comparable to our HAT reactions because ET involves a change in charge, the parallel is clear. The Fe^{III} complexes are more rigid and have fewer low-frequency vibrational modes than Fe^{II}, analogues for both ET and HAT. The large ET entropies support the conclusion that there are substantial vibrational entropy changes for the Fe^{III}/Fe^{II} couples in this system and that $\Delta S°_5$ and $\Delta S°_6$ deviate from zero because of the entropy of the iron HAT half-reactions.

III. Broader Implications. A. Generality of *S*°(AH) ≠ *S*°(A•). The entropy assumption $S°(AH) \approx S°(A^•)$ (eq 15) appears to hold for organic molecules. This is based on the gas-phase data in Table 5 and on well-benchmarked solution studies with a wide range of organic compounds.[20−22] This assumption fails for the iron complexes due to their large number of low-frequency vibrational modes that change upon oxidation or reduction by HAT. It appears that organic compounds have fewer low-frequency modes ($\nu \approx kT$) and/or that few of these modes change substantially upon gain/loss of H•, perhaps due to more localized covalent bonding in organic species compared to more dative bonding in coordination complexes. More studies are needed to determine how general these large entropy changes are for coordination compounds. At the present time, we can only speculate that HAT entropy changes of vibrational origin should often parallel entropies for related electron-transfer half-reactions.

Large entropies are common for Fe^{III}/Fe^{II} redox couples and are smaller for second- and third-row transition metals, as in the Ru^{III}/Ru^{II} redox couples.[56e,j] In general, half-reaction entropies will be large for cases where the orbital occupancy of strongly bonding or antibonding orbitals changes upon reduction of the metal center. This is most noticeable in cases where the spin state changes as well as the oxidation state, the classic example being low-spin Co^{III}/high-spin Co^{II}.[55] Sutin and Weaver have also shown that $\Delta S°$ for ET half-reactions is monotonic with the Marcus self-exchange reorganization energy, λ (a free energy parameter).[58] The inner-sphere component of the reorganization energy involves changes in equilibrium bond lengths. When the metal−ligand bonds become shorter and stronger, the whole complex becomes stiffer, shifting the more entropically relevant low-frequency modes. This is parallel to the vibrational entropy basis for HAT entropies advanced here. If this ET/HAT parallel holds, the ET reorganization energies[59] suggest that large entropy changes may be characteristic of many first-row transition-metal HAT couples. Even just considering

Scheme 2

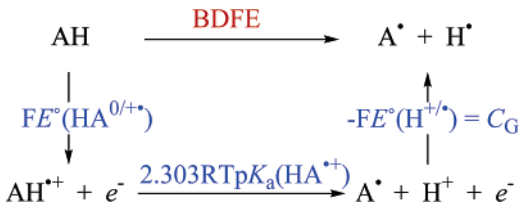

Fe^{III}/Fe^{II} couples, there are a large number of systems in coordination chemistry and in biology where the importance of entropy needs to be evaluated. In contrast, large entropic changes do not appear to be characteristic of organometallic systems, such as metal−carbonyl hydrides.[23] Perhaps organometallic compounds resemble organic molecules in that the more covalent bonding leads to fewer low-frequency modes that are effected by changes in the metal oxidation state.

B. Bond Dissociation Enthalpies (BDEs) from pK_a and $E_{1/2}$ Values. In recent years, many groups, including ours, have used thermochemical cycles to determine A−H bond dissociation enthalpies (BDEs) from measurements of acidity (pK_a) and redox potential ($E_{1/2}$). This approach was used early on by Wiberg, by Eberson, and by Breslow;[19] its popularity dates to its development and extensive use by Bordwell and coworkers.[20−24] One variation of the thermochemical approach is outlined in Scheme 2 and eq 17. The bond dissociation free

$$\mathrm{BDFE[AH]} = -FE°[\mathrm{HA}^{+•/0}] + 2.303RT\mathrm{p}K_a[\mathrm{HA}^{•+}] + C_G \quad (17)$$

energy (BDFE) of A−H is given by its oxidation potential ($-E°[AH^{•+/0}]$), the acidity of the corresponding radical cation ($pK_a[AH^{+•}]$), and the free energy to form a solvated hydrogen atom from the proton and electron in solution ($-FE°[H^{+/•}]$). An analogous cycle involving $pK_a[AH]$ and $E°[A^{0/-}]$ is equivalent. Note that BDFE and BDE are used here as solution quantities, while by strict definition, they should involve only gas-phase species. Bordwell and others have used Scheme 2 and related cycles to provide gas-phase energetics, but this involves additional assumptions about solvation energies and is beyond the scope of this paper.[60]

The pK_a and E values are free energies measured in solution under a specific set of conditions (ideally the same conditions of solvent, temperature, electrolyte, ionic strength, etc.). The $nFE°(H^{+/•})$ term, while specific to these conditions and reference electrode, is valid for all A−H compounds and is, therefore, termed a constant, C_G (the G implying free energy). However, such cycles are typically used to derive enthalpies (BDEs). The BDE is the BDFE plus the entropy change (eq 18). Equation 18 contains the difference between the entropies of AH and A• ($T\Delta S°[AH] - T\Delta S°[A^•]$). When this difference is close to zero — the entropy assumption of eq 15 above — eq 18 reduces to eq 19 where the enthalpy constant C_H includes only $-FE°(H^{+/•})$ and $T\Delta S[H^•]$. C_H has been calculated from thermochemical values, as suggested here, or by fitting eq 19 to

(58) Sutin, N.; Weaver, M. J.; Yee, E. L. *Inorg. Chem.* **1980**, *19*, 1096−1098.
(59) (a) Wherland, S. *Coord. Chem. Rev.* **1993**, *123*, 169−199. (b) Eberson, L. *Electron Transfer Reactions in Organic Chemistry*; Springer-Verlag: Berlin, Germany, 1987.
(60) Complications in determining gas-phase energetics from cycles like Scheme 2 arise when A−H is a strong hydrogen bond donor and significant hydrogen bonding to solvent is present. Leading references include: (a) Mulder, P.; Korth, H.-G.; Pratt, D. A.; DiLabio, G. A.; Valgimigli, L.; Pedulli, G. F.; Ingold, K. U. *J. Phys. Chem. A* **2005**, *109*, 2647−2655. (b) dos Santos, R. M. B.; Simões, J. A. M. *J. Phys. Chem. Ref. Data* **1998**, *27*, 707−739.

known BDEs.[61]

$$\mathrm{BDE[AH]} = \mathrm{BDFE[AH]} - T\Delta S^\circ[\mathrm{AH}] + T\Delta S^\circ[\mathrm{A^\bullet}] + T\Delta S^\circ[\mathrm{H^\bullet}] \quad (18)$$

$$\approx FE^\circ(\mathrm{HA}^{0/+\bullet}) + 2.303RT\mathrm{p}K_{(\mathrm{HA}^{\bullet+})} + C_\mathrm{H} \quad (19)$$

$$C_\mathrm{H} = C_\mathrm{G} + T\Delta S^\circ[\mathrm{H^\bullet}] \quad (20)$$

For the iron HAT redox couples **$Fe^{II}(H_2bip)$**/**$Fe^{III}(Hbip)$** and **$Fe^{II}(H_2bim)$**/**$Fe^{III}(Hbim)$**, the assumption that $S^\circ(\mathrm{AH}) \approx S^\circ(\mathrm{A^\bullet})$ does not hold. In MeCN, S°[**$Fe^{III}(HL)$**] − S°[**$Fe^{II}(H_2L)$**] is −30 cal mol^{-1} K^{-1} for each couple, corresponding to $T\Delta S^\circ = -9$ kcal mol^{-1} in free energy at 298 K. In previous papers, we were unaware of this entropy effect and thus calculated erroneous BDEs using eq 19. The correct BDEs for **$Fe^{II}(H_2bip)$** and **$Fe^{II}(H_2bim)$** are 62 ± 1 and 67 ± 2 kcal mol^{-1}, respectively. Calorimetric studies are underway to obtain more direct measures of these values.

Since the measured pK_a and $E_{1/2}$ values are free energies, it seems prudent to derive BDFEs and avoid assumptions about entropy, particularly for coordination complexes. For compounds where $S^\circ(\mathrm{AH}) \approx S^\circ(\mathrm{A^\bullet})$, as for organic species, the BDE will differ from the BDFE by $\Delta S^\circ[\mathrm{H^\bullet}]$ (eq 21). $T\Delta S^\circ[\mathrm{H^\bullet}]$ varies only slightly with solvent, 4.62 (MeCN), 4.60 (DMSO), 4.78 (toluene), 4.87 (1,2-dichloroethane), and 2.96 (H_2O) at 298 K in kcal mol^{-1}.[62] When $S^\circ(\mathrm{AH}) \approx S^\circ(\mathrm{A^\bullet})$,

$$\mathrm{BDFE} = \mathrm{BDE} - T\Delta S^\circ[\mathrm{H^\bullet}] \quad (21)$$

C. Implications for Rate/Driving Force Correlations for HAT Reactions. The Bell−Evans−Polanyi correlation of activation energies with enthalpic driving force (eq 2) has been a cornerstone of organic radical chemistry for almost 70 years.[1a] The results described here suggest that it should be formulated in free energy terms rather than enthalpic ones, correlating $\Delta G^\ddagger$ with ΔG° or log$k$ with logK_{eq}. We have previously described a number of correlations of log$k$ with BDE for transition-metal HAT reactions, including those of **$Fe^{III}(Hbim)$**.[2,6,13,14] It is now clear that these were, in effect, correlations with BDFEs because the bond energies were derived from pK_a and $E_{1/2}$ values. The bond energies used in these correlations should all be reduced by 5 kcal mol^{-1} to actually be BDFEs, due to the difference between C_G and C_H (eq 20). This correction does not affect the quality of our previous correlations because it does not affect the relative BDFEs; it only shifts the absolute scale. However, because of the entropy issues discussed here, if the accurate BDEs for **$Fe^{II}(H_2L)$** [taking into account $S^\circ(\mathrm{Fe^{II}(H_2L)})$ − S°(**$Fe^{III}(HL)$**)] were used instead of the BDFEs, the correlations would not hold. Similarly, in our application of the Marcus cross relation to reactions of **$Fe^{III}(Hbim)$** and **$Fe^{III}(Hbip)$**, the calculated equilibrium constants are accurate because they were derived from the pK_a and $E_{1/2}$ values and the organic BDEs.[63]

Most rate/driving force correlations in chemistry are linear free energy relations (LFERs)[64] rather than correlations with enthalpies; therefore, perhaps this result is not surprising. The long and varied success of the Polanyi relation is seen, in this light, as a special case, valid only when entropic effects are small.[11a] Its success also supports the suggestion that entropic effects are minor for organic HAT reactions. In the more general case, for instance when metal complexes are involved, a free-energy-based approach such as Marcus Theory is more appropriate.

Conclusions

Hydrogen atom transfer (HAT) reactions from the iron complexes **$Fe^{II}(H_2bip)$** and **$Fe^{II}(H_2bim)$** to the organic radical TEMPO have large negative ground-state entropy changes, $\Delta S^\circ = -30 \pm 2$ cal K^{-1} mo1^{-1} for both. These values are determined from equilibrium constants as a function of temperature using the van't Hoff equation. The K_{eq}'s have been determined by static experiments and from the ratio of forward and reverse bimolecular rate constants. They are independent of concentration and ionic strength, indicating that the large entropy changes are not due to a change in the number of particles (i.e., not due to translational entropy). Similar ΔS° values are observed in acetone and CH_2Cl_2, indicating that neither solvent effects nor hydrogen bonding are the origin of these entropy changes. The high-spin/low-spin equilibria of **$Fe^{II}(H_2bip)$** and **$Fe^{III}(Hbip)$** are also not responsible. Computational studies and analogies with related electron-transfer and spin equilibria indicate that the primary contribution is from vibrational entropy. Many low-frequency vibrational modes shift to higher energy upon oxidation of Fe^{II} to Fe^{III}. A similar ΔS° is also observed for the **$Fe^{III}(H_2bim)$**/**$Fe^{II}(H_2bim)$** electron-transfer half-reaction based on its reaction with CpCp*Fe.

The $\Delta S^\circ = -30 \pm 2$ cal K^{-1} mo1^{-1} is a substantial value, corresponding to $T\Delta S^\circ = -9$ kcal mol^{-1} at 298 K (a change in K_{eq} of 4×10^6). This large entropy change contradicts the common assumptions that $\Delta S^\circ \approx 0$ for HAT reactions and that, for a half-reaction, $\mathrm{AH} \rightarrow \mathrm{A^\bullet} + \mathrm{H^\bullet}$, $\Delta S^\circ(\mathrm{AH}) \approx \Delta S^\circ(\mathrm{A^\bullet})$. While the generality of this result is currently being explored, we conclude that analyses which use these entropy assumptions should be applied with care when metal complexes are involved. This includes the derivation of bond dissociation enthalpies (BDEs) from pK_a and $E_{1/2}$ measurements via the Bordwell method and the correlation of rates with BDE. In both cases, it is more appropriate to use bond dissociation free energies (BDFE) rather than enthalpies.

Experimental Section

General Considerations. All manipulations were carried out under anaerobic conditions using standard high-vacuum line and nitrogen-

(61) An excellent discussion on the derivation of C_G and C_H is provided in (a) Tilset, M. The Thermodynamics of Organometallic Systems Involving Electron-Transfer Paths. In *Electron Transfer in Chemistry*; Balzani, V., Ed.; Wiley-VCH: New York, 2001, Vol. 2, pp 677−713. (b) Mayer, J. M. In *Biomimetic Oxidations Catalyzed by Transition Metal Complexes*; Meunier, B., Ed., Imperial College Press: London, 2000; pp 1−43.

(62) $\Delta S^\circ[\mathrm{H^\bullet}] = S^\circ_f[\mathrm{H^\bullet}]_g + \Delta S^\circ_{solvation}[\mathrm{H^\bullet}]$; see supporting information for details. (a) $S^\circ_f[\mathrm{H^\bullet}]_g = 27.419$ cal mol^{-1} K^{-1}; NIST Chemistry WebBook. NIST Standard Reference Database 69. http://webbook.nist.gov/chemistry/ (June 2005 release). (b) $\Delta S^\circ_{solvation}[\mathrm{H^\bullet}]$ is approximated by the solvation entropy of H_2 in the same solvent; see: Roduner, E.; Bartels, D. M. *Ber. Bunsen-Ges. Phys. Chem.* **1992**, *96*, 1037−1042. (c) $\Delta S^\circ_{solvation}[H_2]$ in MeCN and toluene; see: Brunner, E. *J. Chem. Eng. Data* **1985**, *30*, 269−273. (d) $\Delta S^\circ_{solvation}[H_2]$ in H_2O, DMSO, and 1,2 dichloroethane; see: Hydrogen and Deuterium. In *IUPAC, Solubility Data Series*; Young, C. L., Ed.; Pergamon Press: New York, 1981; Vols. 5/6, pp 259, 239.

(63) Both values should have been reduced by 5 kcal mol^{-1} to make them true BDFEs (eq 20). However, since K_{eq} requires the difference between **$Fe^{II}(H_2L)$** and the organic BDE, this correction cancels out, yielding the correct K_{eq}. This would not be the case, for instance, if our measurement of the BDE for **$Fe^{II}(H_2L)$** had been done using calorimetry, which does not account for S°(**$Fe^{II}(H_2L)$**) − S°(**$Fe^{III}(HL)$**). In this case, the resulting ΔBDE would yield an ΔH° value, not ΔG°.

(64) Lowry, T. H.; Richardson, K. S. *Mechanism and Theory in Organic Chemistry*; Harper & Row Publishers: San Francisco, CA, 1976; Chapter 2.

filled glovebox techniques, unless otherwise noted. NMR spectra were acquired on Bruker Avance-500, DRX-499, Avance-300, or Avance-301 spectrometers. Static UV−visible spectra were obtained using a Hewlett−Packard 5483 spectrophotometer equipped with an eight-cell holder thermostated with a Thermo-Neslab RTE-740 waterbath. Spectra are reported as λ_{max}, nm [ϵ, M^{-1} cm^{-1}]. Air-sensitive samples were prepared in the glovebox, and their spectra were taken using either quartz cuvettes attached to Teflon-stoppered valves (Kontes) or injectable screw-capped cuvettes with silicone/PFTE septa (Spectrocell). Septa were replaced after each experiment. Rapid kinetic measurements were taken using an OLIS USA stopped-flow instrument equipped with the OLIS rapid-scanning monochromator and a UV−vis detector and thermostated by a Neslab RTE-111 waterbath.

Materials. Low water content CH_3CN (<10 ppm H_2O; Allied Signal/Burdick and Jackson brand) was taken from a keg sparged with argon and dispensed through the glovebox. Deuterated solvents (Cambridge Isotopes Laboratories) were dried and stored in the glovebox. CD_3CN was dried by stirring overnight with CaH_2, vacuum transferring, stirring briefly (<1 h) over P_2O_5, vacuum transferring back over CaH_2 for ca. 30 min, and then storing free of drying agent. Acetone was dried by stirring over $CaSO_4$. CH_2Cl_2 was dried over CaH_2 before use and stored in the glovebox freezer, wrapped in Al foil. Other solvents were dried using a Grubbs-type Seca Solvent System installed by GlassContour.[65] 2,2,6,6-Tetramethyl-1-piperidinyloxy (TEMPO; Acros Organics and Aldrich) was sublimed at room temperature under static vacuum before use. $^nBu_4NClO_4$ (99% Acros) was recrystallized twice from boiling absolute EtOH and dried overnight under dynamic vacuum.[66] Triflic acid (99%) was purchased from Acros Organics and stored in the glovebox freezer. All other reagents were purchased from Aldrich and used as received.

Iron Complexes. Iron(II) tris[2,2′-bi-1,4,5,6-tetrahydropyrimidine]-[perchlorate] ($[Fe^{II}(H_2bip)_3][ClO_4]_2$, **$Fe^{II}(H_2bip)$**); $[Fe^{III}(H_2bip)_2(Hbip)]$-$[ClO_4]_2$, (**$Fe^{III}(Hbip)$**); $[Fe^{III}(H_2bip)_3][ClO_4]_3$, (**$Fe^{III}(H_2bip)$**); iron(II) tris[2,2′-bi-2-imidazoline][perchlorate] ($[Fe^{II}(H_2bim)_3][ClO_4]_2$, (**$Fe^{II}(H_2bim)$**); $[Fe^{III}(Hbim)(H_2bim)_2][ClO_4]_2$, (**$Fe^{III}(Hbim)$**); and $[Fe^{III}(H_2bim)_3]$-$[ClO_4]_3$, (**$Fe^{III}(H_2bim)$**) were prepared and characterized following the procedures described in Yoder et al.[25] *Caution: The perchlorate salts used herein are explosive and should be handled with care in small quantities only. They should not be heated when dry or subjected to friction or shock, such as scratching with a non-Teflon-coated spatula.*

CpCp*Fe was prepared from $FeCl_2$ following the procedure of Manriquez et al.[67] and purified by sublimation at 40 °C under static vacuum. UV (MeCN): 432 [120].

$[CpCp^*Fe]PF_6$[37] was quantitatively generated in MeCN by addition of a stoichiometric amount of 8.1 mM $[N(tolyl)_3][PF_6]$[5e] to 3.3 mM CpCp*Fe. UV (MeCN): 740 [350], 600 [160].[37]

TEMPO-H. The literature preparation of 2,2,6,6-tetramethyl-1-hydroxypiperidine (TEMPO-H)[30] was modified to give better yield and purity. A solution of TEMPO (2.0 g, 13 mmol) in 30 mL of 1:1 deionized water/acetone was sparged with N_2 for ∼15 min. Under flowing N_2, excess $Na_2S_2O_4$ (3.8 g, 22 mmol) was added, and the suspension was stirred until the orange color was no longer visible (ca. 10 min). Acetone was then pumped off under dynamic vacuum to yield a thick white suspension. Prolonged pumping caused a reduction in yield, as the TEMPO-H also sublimed. The product was extracted from the aqueous layer with Et_2O (5 × 10 mL) by PFTE cannula, maintaining a N_2 atmosphere. The Et_2O was then removed under dynamic vacuum. Any residual water was removed by additional dissolution and subsequent evaporation cycles in dry Et_2O as needed. Purification by sublimation at room temperature to a cold finger cooled with dry ice/acetone gave 1.5 g of white crystalline TEMPO-H (74%). ^1H NMR (CD_3CN): δ 1.06 (s, 12H), 1.45 (s, 6H), 5.3 (br s, 1H).

Crystal Structures. Detailed structural information is available in the Supporting Information.

UV−Vis Stopped-Flow Kinetics. In the glovebox, a 0.1 mM **$Fe^{II}(H_2bip)$** solution and 4−5 solutions of TEMPO (3−80 mM, to ensure pseudo-first-order conditions) were prepared in CH_3CN and loaded into syringes. These were removed from the glovebox in pairs and immediately attached to the stopped-flow to minimize exposure to air. The system was thermally equilibrated for 15−25 min before data acquisition. A minimum of six kinetic runs were done at each TEMPO concentration and temperature. Typical spectra and kinetic fit are shown in Figure S2. Kinetic data were analyzed using the OLIS SVD global fitting software, averaging the ≥6 k_{obs} determinations for each temperature and concentration. The linear regressions of k_{obs} versus [TEMPO] (Figure S1) and the Eyring and van't Hoff plots were done in Kaleidagraph, weighting each rate constant with its associated standard deviation. Reported errors were double the fully propagated standard deviations. The reactions **$Fe^{III}(Hbip)$** (0.1 mM) + TEMPO-H (3−50 mM) and **$Fe^{III}(Hbim)$** (2.1×10^{-5} M) + TEMPO-H (16−520 equiv) were measured in the same fashion (Figures S4 and S5). Solutions with high concentrations of TEMPO-H gradually formed tetramethylpiperidine, which slowed the kinetics; therefore, only freshly made solutions were used.

$Fe^{II}(H_2bim)$ + TEMPO kinetics were run under second-order approach to equilibrium conditions with a large excess of TEMPO. This was necessary because of the substantially unfavorable K_{eq}. Measurements followed the procedure given earlier in this paper, using 60−80 μM solutions of **$Fe^{II}(H_2bim)$** and five TEMPO stock solutions (80−500 mM). Using SPECFIT global analysis software,[34] the data were fit to a reversible second-order kinetic model with rate constants k_6 and k_{-6}. Fe^{II}, Fe^{III}, and TEMPO were defined as colored, and Fe^{II} and TEMPO had nonzero initial concentrations. Both the TEMPO spectrum and the values of k_{-6} were fixed in this fitting procedure, and the rate constant k_6 was iteratively refined. The extracted k_6 are independent of [TEMPO] (Figures S6, S7). The average was taken over all concentrations, and the reported errors are twice the standard deviation of the set.

Static Equilibria Measurements. For each of the following cases, the relevant extinction coefficients were determined as a function of temperature and solvent using Beer's Law plots on multiple independent samples (Table S4).

$Fe^{II}(H_2bip)$ + TEMPO ⇄ $Fe^{III}(Hbip)$ + TEMPO-H. Individual stock solutions of 50−200 μM **$Fe^{II}(H_2bip)$**, ∼240 mM TEMPO, and ∼160 mM TEMPO-H were prepared in the glovebox. A UV−vis cuvette sealed with a septum was charged with 2.0 mL of **$Fe^{II}(H_2bip)$** stock solution and thermally equilibrated in the spectrophotometer for 20 min. A large excess of TEMPO (ca. 130 equiv) and then a series of aliquots of TEMPO-H (up to 500 equiv) were sequentially added through the septum by syringe, with a spectrum taken after each addition, Figure S3. The additions were done as quickly as possible, and various control experiments showed no measurable air oxidation of **$Fe^{II}(H_2bip)$** to **$Fe^{III}(Hbip)$**.[26] Each spectrum was deconvoluted into the component absorbances of **$Fe^{III}(Hbip)$**, **$Fe^{II}(H_2bip)$**, and TEMPO (TEMPO-H has no significant absorbance in the relevant UV−vis region) using a matrix application of Beer's Law in Microsoft Excel.[68] The resulting K_{eq}'s were then averaged to give a single value for each cuvette (Table S1), with multiple cuvettes measured at each temperature.

$Fe^{II}(H_2bim)$ + TEMPO ⇄ $Fe^{III}(Hbim)$ + TEMPO-H. Following the method given earlier in this paper, up to 0.13 equiv of **$Fe^{II}(H_2bim)$** (using a 20 mM stock solution) was added in 50 μL increments to a thermally equilibrated cuvette containing 2 mL of 30 mM TEMPO in MeCN. In this approach, the change in absorbance at 676 nm is due

(65) Pangborn, A. B.; Giardello, M. A.; Grubbs, R. H.; Rosen, R. K.; Timmers, F. J. *Organometallics*, **1996**, *15*, 1518 −1520; see also http://www.glass-contour.com/index.html
(66) Perrin, D. D.; Armarego, W. L. F. *Purification of Laboratory Chemicals*, 3rd ed.; Pergamon Press: New York, 1989; p 280.
(67) Manriquez, J. M.; Bunel, E. E.; Oelckers, B. *Inorg. Synth.* **1997**, *31*, 214−217.
(68) Least Squares Methods for Multivariate Data. In *User Manual SPECFIT/32*; Spectrum Software Associates: Marlbourough, MA, 2000−2001; pp 95−96.

solely to **Fe^{III}(Hbim)**, rather than the strongly absorbing TEMPO background. The data analysis converted this ΔA_{676} to [**Fe^{III}(Hbim)**], from which the other equilibrium concentrations were derived by mass balance. Plots of [**Fe^{III}(Hbim)**]^2 versus [**Fe^{II}(H_2bim)**] are linear (Figure S11 and S12), with the slope being K_{eq} × [TEMPO] ([TEMPO] is essentially constant under these conditions).

Fe^{III}(H_2bim) + CpCp*Fe ⇄ Fe^{II}(H_2bim) + [CpCp*Fe]$^+$. Again following the method discussed in the preceding sections, a septum-sealed cuvette was charged with 0.07 g (0.2 mmol) of Bu_4NClO_4, 2 mL of 2.0 mM **Fe^{III}(H_2bim)** (4.7 μmol), and 250 μL of 1.2 mM HOTf (0.3 μmol; added to remove trace **Fe^{III}(Hbim)**[69]). Once the cuvette was thermally equilibrated, aliquots of 7.4 mM CpCp*Fe (0−0.31 equiv) were added, and the formation of CpCp*Fe^+ at 740 nm was observed. Addition of **Fe^{II}(H_2bim)** (1.1 μmol, 0.23 equiv) shifted the equilibrium back toward CpCp*Fe. Data analysis was the same as that for **Fe^{II}(H_2bim)** + TEMPO using the absorbance at 740 nm due to [CpCp*Fe]$^+$, Figure S10.

(69) Samples of **Fe^{III}(H_2bim)** always appeared to contain trace amounts (< 1%) of **Fe^{III}(Hbim)**. Based on the UV-vis absorbance of **Fe^{III}(Hbim)** at 676 nm, 1 equiv of HOTf was added to fully protonate the sample to **Fe^{III}(H_2bim)**. Excess HOTf resulted in decomposition of **Fe^{III}(H_2bim)**.

Acknowledgment. We gratefully acknowledge financial support from the U.S. National Institutes of Health (Grant GM50422) and from the Natural Science and Engineering Research Council of Canada (NSERC PGS D2). The authors are also indebted to Dr. A. G. DiPasquale for the X-ray crystal structures, to Drs. J. P. Roth, J. C. Yoder, and T. J. Won for their prior studies on these systems, and to others (too many to name) for valuable discussions.

Supporting Information Available: Detailed spectral, rate, equilibrium, X-ray, and calculated data are provided. This material is available free of charge via the Internet at http://pubs.acs.org.

JA0686918